Ab initio Investigations into the Geometry and Electronic Excitations of Novel Ruthenium Chloride Clusters

by

Alexander George Boncheff

A Thesis
presented to
The University of Guelph

In partial fulfillment of requirements
for the degree of
Master of Science
in
Chemistry

Guelph, Ontario, Canada

ABSTRACT

Ab initio INVESTIGATIONS INTO THE GEOMETRY AND ELECTRONIC EXCITATIONS OF NOVEL RUTHENIUM CHLORIDE CLUSTERS

Alexander George Boncheff
University of Guelph, 2011

Advisor:
Professor Mario Monteiro

In efforts to coordinate carbohydrates to transition metal centres, the coordination of D-(+)-Glucosamine to ruthenium was performed. The product from this reaction was a vibrant blue substance that degraded in a characteristic fashion of blue to green to yellow, indistinguishable to that of the ruthenium coordination precursor “Ruthenium Blue”. The MALDI-ToF-MS spectra of the blue product and subsequent green and yellow degradation products showed the presence of a series of $[Ru_xCl_y]^-$ ruthenium chloride clusters. Structures of the clusters and their respective electronic excitations were determined using *ab initio* calculations. Calculations were performed using Density Functional Theory and the CIE1931 colour metric was used to process the electronic excitations into a physically perceived colour. The optimized structures that resulted from the *ab initio* calculations had the same physically perceived colour as the species found in the product, and thus could be another possibility into the composition of “Ruthenium Blue”.

TABLE OF CONTENTS

List of Figures *v*

List of Tables *vii*

Chapter 1: Introduction 1

1.1 Motivation 2

1.2 Bacterial Polysaccharides 3

1.3 Coordination of Monosaccharides to Ruthenium 12

1.4 Insight into the Composition of Ruthenium Blue 13

1.5 The CIE1931 Colour Metric 16

1.6 Overview of Research Project 21

Chapter 2: Experimental 24

2.1 Synthetic Strategy 25

2.2 Computational Strategy 25

2.3 Synthesis of Blue Compound 27

2.4 *Ab initio* calculations on Ruthenium Chloride clusters 28

2.5 Processing of Electronic Excitations into UV/Vis spectra 28

2.6 Methods for Mass spectrometry of Ruthenium Chloride clusters 36

Chapter 3: Results and Discussion 37

3.1 Ruthenium Blue Compound 38

3.1.1 Mass Spectrometry results of Blue Compound 39

3.2 *Ab initio* results on Ruthenium Chloride clusters 45

3.3 Calculated Electronic Excitation Spectra of Ruthenium Chloride Clusters 52

3.4 Calculated Electronic Excitation Spectra of the Blue Compound 57

3.5 Calculated Electronic Excitation Spectra of other Ruthenium Halides 60

Chapter 4: Conclusions and Future Work 63

Chapter 5: References 68

Chapter 6: Appendix 72

6.1 Input Files for the TDDFT Calculations of the Ruthenium Chloride Clusters 73

6.2 Cartesian Coordinates of Geometry Optimized Ruthenium Chloride Clusters 81

6.3 Raw UV/Vis Spectra Data for the Ruthenium Chloride Clusters 91

LIST OF FIGURES

Figure 1 – *The structure of the Lipopolysaccharide*

Figure 2 – *Methods for Structural Characterization of Complex Bacterial Polysaccharides*

Figure 3 – *A Carbohydrate Chain Showing the Glycosidic Linkages*

Figure 4 – *Structure of the* $[Ru_5Cl_{12}]^{-2}$ *anion proposed by Rose and Wilkinson. (1970)*

Figure 5 – *Structure of* $[Ru_3Cl_{12}]^{-4}$ *cluster by Bino and Cotton*

Figure 6 – *The 1931 CIE Standard Observer RGB Colour Matching Functions*

Figure 7 – *Matrix Transformation to Convert the CIE1931 RGB Colour Matching Functions into the CIE1931 XYZ Colour Matching Functions*

Figure 8 – *The 1931 CIE Standard Observer XYZ Colour Matching Functions*

Figure 9 – *The CIE1931 Colour Space*

Figure 10 – *Flowchart of the methodology for calculating the perceived physical colour of the ruthenium chloride clusters*

Figure 11 – *Example of Inversion and normalization of electronic excitation spectra using the spectrum of* $[Ru_2Cl_6]^-$

Figure 12 – *Conversion Function for Inversion of the UV/Vis spectrum*

Figure 13 – *Code for Determining the Maximum Value of a Series of Data Points*

Figure 14 – *CIE1931 Colour Matching Functions*

Figure 15 – *Functional for Obtaining the Tristimulus Values from Integration of the Inverted Absorption Spectrum with the CIE1931 Colour Matching Functions from Beck*

Figure 16 – *Normalization function of the Tristimulus Values into Chromacity Coordinates for x and y respectively*

Figure 17 – *CIE1931 Colour Space Metric*

Figure 18 – *Solutions of the blue compound at various stages of decomposition. a) blue, b) green c) yellow*

Figure 19 – *LDI-ToF-MS of $RuCl_3 \cdot 3H_2O$*

Figure 20 – *MALDI-ToF-MS spectra of the Blue Compound at the blue degradation stage. Negative mode*

Figure 21 – *MALDI-ToF-MS spectra of the Blue Compound at the green degradation stage. Negative mode*

Figure 22 – *MALDI-ToF-MS spectra of the Blue Compound at the yellow degradation stage. Negative mode*

Figure 23 – *Experimental (top,blue) and Calculated (bottom, orange) Mass Spectrum Profile of $[Ru_2Cl_6]^-$*

Figure 24 – *Experimental (top,blue) and Calculated (bottom, orange) Mass Spectrum Profile of $[Ru_3Cl_9]^-$*

Figure 25 – *Structures of the Ruthenium Chloride Clusters*

Figure 26 – *UV/Vis spectra of Ruthenium Chloride Clusters. (a) $[RuCl_4]^-$, (b) $[RuCl_5]^-$, (c) $[Ru_2Cl_6]^-$, (d) $[Ru_2Cl_7]^-$, (e) $[Ru_3Cl_8]^-$, (f) $[Ru_3Cl_9]^-$, (g) $[Ru_4Cl_{11}]^-$, (h) $[Ru_5Cl_{12}]^-$*

Figure 27 – *Plot of Chromacity Coordinates of the Clusters on the CIE1931 Gamut*

Figure 28 – *Calculated UV/Vis spectra of the Solutions. (a) Blue and (b) Yellow*

Figure 29 – *Plot of Chromacity Coordinates of the Blue and Yellow Solutions on the CIE1931 Gamut*

Figure 30 – *UV/Vis absorption spectra of a) RuF_4 b) $RuCl_3$ c) $RuBr_3$*

Figure 31 – *RuF_4, $RuCl_3$, $RuBr_3$ plotted on CIE1931 Colour Space*

Figure 32 – *UV/Vis spectrum of the Blue Solution with the Contribution from $[Ru_4Cl_{11}]^-$ highlighted*

LIST OF TABLES

Table 1 – *List of NMR Experiments Used in the Structural Determination of Polysaccharides*

Table 2 – *Composition of the Blue Compound at Various Colours*

Table 3 – *CIE1931 Chromacity Coordinates for the Ruthenium Chloride Clusters*

Table 4 – *CIE1931 Chromacity Coordinates of the Solutions*

Chapter 1: Introduction

1.1 Motivation

Our research focuses on the composition analysis and structural characterization of complex bacterial polysaccharides (PSs). These polysaccharides are highly specific macromolecules that are expressed on the surface of the bacterial cell wall. They are typically comprised of a repeating oligosaccharide unit and are on average 10 repeat units long. The reason for interest in the bacterial PSs is due to the antigenic properties and immunostimulant effects from from these macromolecules which is used in the development of vaccine and drug design. However a full structural and conformational determination must be obtained for research to begin on drug design and vaccine development based on these bacterial PSs. The structural characterization of the polysaccharides is not a trivial process and involves interpreting various convoluted spectra across various analytical methods. In searching for alternative methods, it was thought that by coordinating the hydroxyl or amine moieties of the sugars to metal centres, the spectra used for structural characterization could be simplified making the process easier.

1.2 Bacterial Polysaccharides

Bacteria have the ability of building and expressing polysaccharides on the surface of the cell to suit a variety of functions. Bacterial PSs can be found in various parts of the cell surface and outer membranes such as the peptidoglycan cell wall, the lipopolysaccharide (LPS) layer and bacterial capsule. The LPS and capsule of bacteria are the macromolecules of interest to vaccine and drug development as they have the antigenic and endotoxic properties that “make people sick”. These bacterial polysaccharides are also highly specific and are divided down into strains with certain bacterial species having the number of strains reach into the hundreds. As a result conformational studies are also useful in determining whether or not cross-reactivity between polysaccharides from separate bacterial strains exist, allowing us to develop drugs or vaccines that can be effective across multiple strains of the same bacterial species.

The lipopolysaccharide (LPS) is found on the outer membrane of Gram-negative bacteria and is made up of 3 components: Lipid A, Core and O-Antigen. The a drawn example of the LPS showing the arrangement of the structures is depicted in *Figure 1.*

Figure 1 – The structure of the Lipopolysaccharide[1]

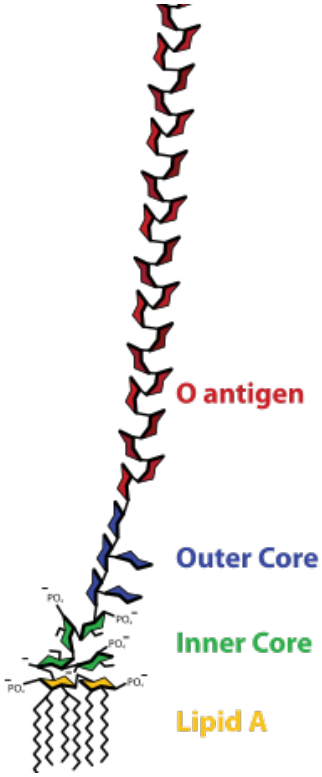

The Lipid A is a glycolipid macromolecule that anchors of the LPS to the outer lipid membrane of a Gram-negative bacteria. The Lipid A is also a powerful endotoxin and immunostimulator and it's effects are implicated in the onset of a Gram-negative bacterial infection. The adjacent structure is the Core which is an oligosaccharide unit that is primarily structural and often contains non-carbohydrate moieties which are necessary for the proper function of the bacterial cell[2]. The Core generally does not have immunostimulatory properties and is not of interest for vaccine or drug development. Our main interest however is in the O-Antigen component. The O-Antigen of the LPS is the macromolecule

that we study for structural characterization. O-Antigens, as their name suggests, have immunostimulant properties and are important in antibody recognition of invading bacterial cells. The general composition of the O-Antigen varies widely from bacterial species to species and from specific strain to strain[3]. As mentioned before, cross-reactivity can be determined between between certain strains of bacteria which allows for the development of multi-valent vaccines.

Certain bacterial species can also produce a bacterial capsule that is expressed as a very loose and jelly-like coating on the outside of the bacterial cell. The capsule is composed of linear branches of polysaccharides with a repeating unit of generally one to six monosaccharides. The capsule protects the bacteria from the immune system by “cloaking” the antigenic sites and preventing antibody recognition of cell surface antigens[4]. Should the bacteria eventually get tagged by the immune system, the jelly-like physical nature of the capsule can be use by the bacteria to “slip away” before being engulfed by the phagocyte. With these properties the sugars present in the bacterial capsule can also be used for vaccine development to protect against infection.

Structural characterization of a PS is a long and time consuming process that is often the main component of a graduate research project. As seen in *Figure 2*, various methods of chemical analysis must be used together in tandem for the full structural characterization. The process for PS characterization starts with a sugar composition analysis to determine the individual monosaccharide units that make up the macromolecule. Using GC-MS and the Alditol Acetate procedure[5] for carbohydrates, signature fragmentation patterns of known monosaccharide standards are compared to those separated by the GC-MS. The next step is to determine the glycosidic linkages and their positions through Partially Methylated Alditol Acetate experiments and GC-MS[6]. At this point we have a knowledge of glycosidic linkage sites for the monosaccharides of the PS and a crude chain of the PS can be determined. Determining the anomeric conformation of the monosaccharide units gives us information on the overall structure of the entire PS. Various Nuclear Magnetic Resonance (NMR) experiments need to be performed in order to get a picture of the entire conformation of the PS. Conformational analysis starts with 1D ^{1}H-NMR which gives information on the presence of alpha- and beta-conformation monosaccharides as well as the chemical shift of the ring protons of the monosaccharide units. A list of the 2D NMR experiments that are used and what information is determined from the resulting spectra are listed below in *Table 1*.

Table 1 – List of NMR Experiments Used in the Structural Determination of Polysaccharides[7]

List of Experiments	*Information Obtained*
Correlation spectroscopy (COSY)	Able to correlate ^{1}H-^{1}H nuclei that are J-coupled to each other. Contains information about dihedral angles
Total correlation spectroscopy (TOCSY)	Able to correlate a protons that are spin coupled together in a spin system. For carbohydrates a spin system constitutes an individual monosaccharide. Able to differentiate protons within a monosaccharide unit.
Heteronuclear single-quantum correlation spectroscopy (HSQC)	Able to correlate individual heteronuclear-^{1}H nuclei through a single bond. Useful for determining bonding between protons and heteronuclei
Heteronuclear multiple-bond correlation spectroscopy (HMBC)	Able to correlate individual heteronuclear-^{1}H nuclei over a longer range than HSQC, typically over 2-4 bonds.
Nuclear Overhauser effect spectroscopy (NOESY)	Able to correlate ^{1}H-^{1}H nuclei through space, typically across 2-4Å. Useful in determining conformational shape of the polysaccharide.

Figure 2 – Methods for Structural Characterization of Complex Bacterial Polysaccharides

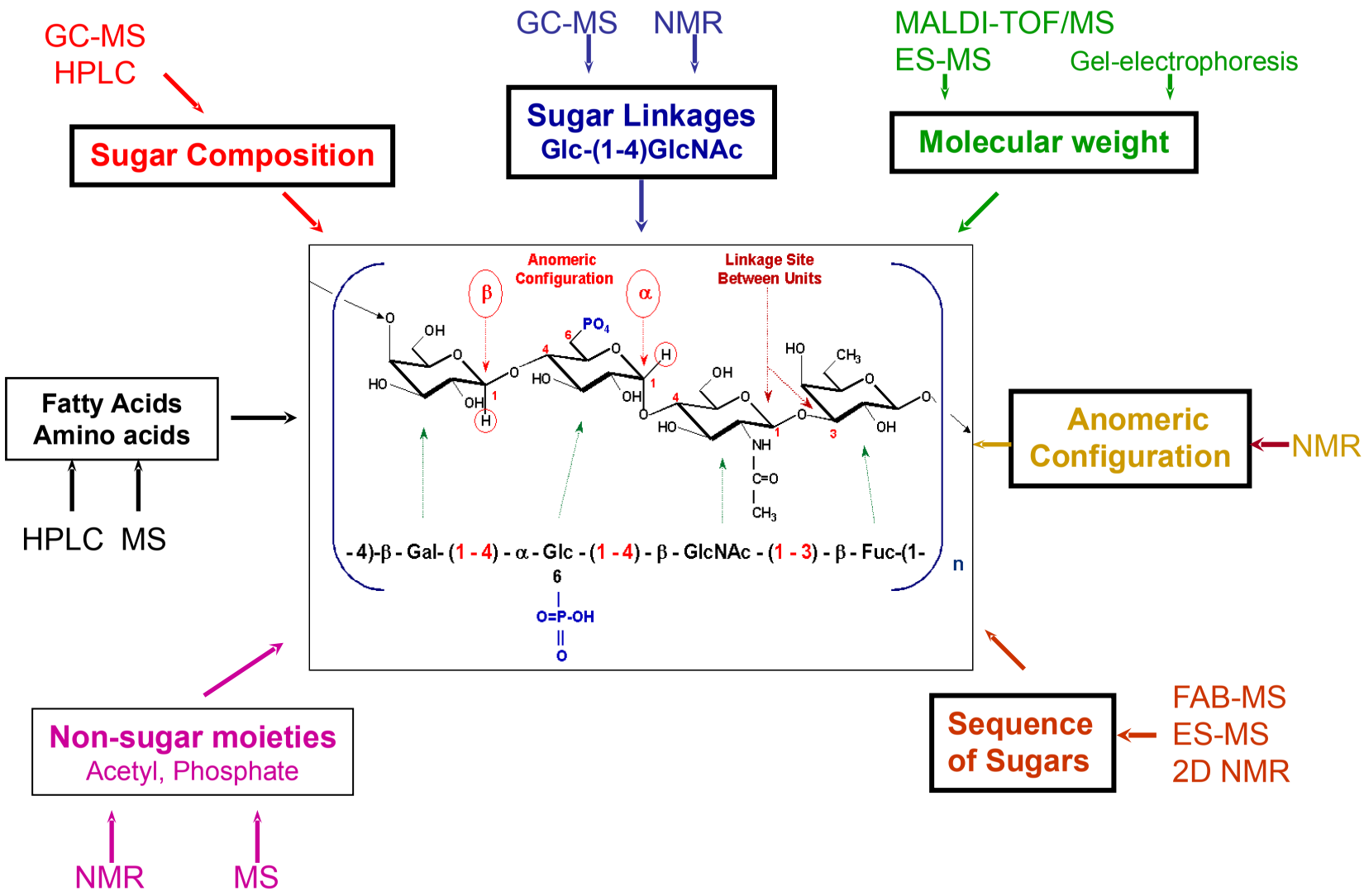

One can see that the structural characterization process for determining the structure of carbohydrates is not a trivial process given how many experiments and spectra need to be analyzed in tandem. An easy method for bypassing spectroscopic determination would be to employ x-ray crystallography similar to that used for protein analysis. However x-ray crystallography is generally not possible for carbohydrates for good reason. Within the polysaccharide, the glycosidic bonds of the carbohydrate chain are very flexible and have a high degree of rotation. A polysaccharide chain contains three types of glycosidic bonds that can rotate:

C-C-O-C, C-O-C-C and O-C-O-C (present only in 1-6 linkages) which are denoted as φ, ψ and ω respectively[8]. These degrees of rotation can be seen in *Figure 3*.

Figure 3 – A Carbohydrate Chain Showing the Glycosidic Linkages.[8]

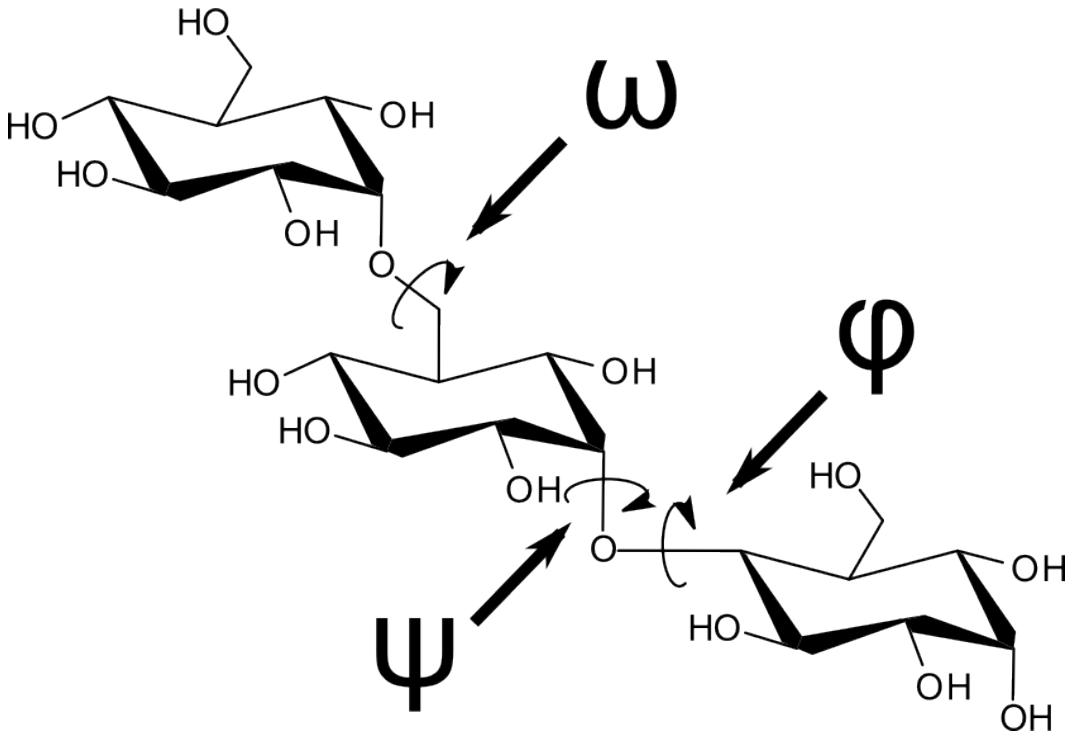

This high degree of mobility of the glycosidic bonds prevents the carbohydrate from being successfully crystallized for x-ray crystallography as compared to protein structures. As a result structural characterization and conformation must be determined via mass spectrometry and nuclear magnetic resonance (NMR) experiments. We envisaged that the coordination of the PSs to ruthenium, through amine and hydroxyl moieties, may help us obtain less convoluted NMR spectra of the PSs though downshifting of the chemical shift of the coordinating atoms. Additionally, higher resolution of the spectra could be obtained due to decreased flexibility and rotation of the coordinated PS. It was also thought that this decrease in the flexibility of the polysaccharide would

promote the possibility of yielding compounds suitable for crystallographic analysis.

The coordination of monosaccharide units to transition metals, especially those of the platinum group, is well-documented in the literature[9],[10]. X-ray crystal structures have also been obtained from the products formed in the coordination reactions. Other investigations into the mechanisms of coordination, with full characterization of the resulting products, have also been carried out with metals such as iron[11], platinum[12], palladium[12], and copper[13]. X-ray crystallography and spectroscopic data has demonstrated that monosaccharides coordinate to the metal through vicinal hydroxyl or amine functional groups. While there are no literature examples of the coordination of monosaccharide carbohydrates to ruthenium, it has been shown that other platinum group metals have been successful and thus ruthenium coordination should be similar. If coordination of monosaccharides to ruthenium proved to be successful, then successive studies into the coordination of the full bacterial polysaccharide to ruthenium would then be investigated. Due to the relatively high monetary cost of obtaining bacterial polysaccharides, ruthenium was chosen as the coordination centre in order to maintain cost-effectiveness of this study as it is the cheapest of the platinum group metals at the time of publication.

1.3 Coordination of Monosaccharides to Ruthenium

Our first investigations into the coordination of polysaccharides to transition metals involved reacting D-(+)-Glucosamine with $RuCl_3 \cdot 3H_2O$. Glucosamine was used as the monosaccharide of choice due to the presence of the amine moiety which is common to the PSs within our field of research. Using glucosamine would have also given insight into bonding preference to ruthenium through vicinal amine-hydroxyl or vicinal hydroxyl-hydroxyl groups. The method of coordination was to use the coordination precursor “Ruthenium Blue” to synthesize a monosaccharide-ruthenium complex. From this reaction, a product that was moderately air and water stable was isolated as an intense blue solid. The colour of the product in solution was visually similar to that of original coordination precursor Ruthenium Blue.

Ruthenium Blue is a versatile starting material for creating ruthenium coordination complexes[14]. G. Wilkinson showed that a wide variety of complexes can be formed by the simple addition of a ligand to an aqueous solution of Ruthenium Blue. Throughout the literature various methods exist for the synthesis of Ruthenium Blue. Rose and Wilkinson used a hydrogen/platinum reduction in ethanol[15] while Mercer and Dumas used an acidic solution of Potassium Ruthenium Chloride and reduction using electrochemistry to produce the vibrant blue solution[16]. A much simpler method for obtaining Ruthenium Blue,

taken from Togano et al., can be made by refluxing $RuCl_3 \cdot 3H_2O$ in ethanol under an inert atmosphere[17]. The progress of the synthesis can be tracked by the signature colour change from the original yellow/brown of $RuCl_3 \cdot 3H_2O$ solution, to green, to the final blue colour. This colour change takes place over approximately 5-6 hours. If exposed to air the Ruthenium Blue solution degrades within minutes to the original green colour followed by the original yellow colour 90 minutes later. This high level of air sensitivity makes studying Ruthenium Blue cumbersome via commonly used analytical techniques. The colour changes seen in the solutions of Ruthenium Blue upon exposure to air are also seen in the formation and degradation of the blue compound formed from $RuCl_3 \cdot 3H_2O$ and D-(+)-Glucosamine, but the degradation is slower (approximately 7 days).

1.4 Insight into the Composition of Ruthenium Blue

Since the discovery of Ruthenium Blue, various literature reports on the composition of the vibrant blue solution have been proposed. These reports describe a wide range of possibilities and conclusions, ranging from single species[18] to multispecies solutions[15], ionic (both positive[16] and negatively[18] charged) and neutral species. Additionally, the studies report ruthenium in varying oxidation states from +4 to +2 oxidation state with +4 and +2 being the most commonly reported. As well a wide range of analytical techniques such as chromatography, voltammetry, X-ray crystallography with co-compounds for

assisting in crystalization and various methods of mass spectrometry have been employed to determine the structure of Ruthenium Blue.

A few of the notable reported results are as follows. In 1970, Rose and Wilkinson published results reporting a $[Ru_5Cl_{12}]^{-2}$ cluster with varying oxidation states for ruthenium ranging from +4 to +2[15]. $[Ru_5Cl_{12}]^{-2}$ was isolated as a deep blue salt with (*o*-phenylenedimethylene) bis(triphenylphosphonium) as a counter-ion. Elemental analysis and x-ray powder diffraction was used to determine the composition and structure, shown in *Figure 4*.

Figure 4 – Structure of the $[Ru_5Cl_{12}]^{-2}$ anion proposed by Rose and Wilkinson. (1970)

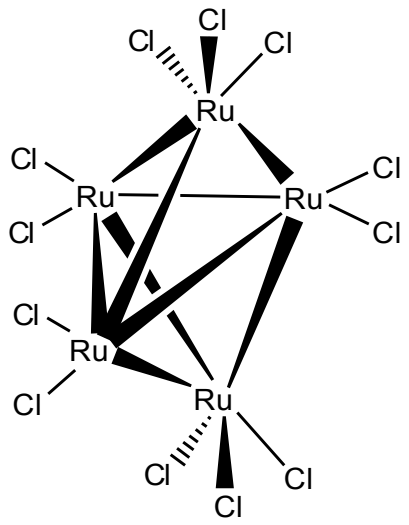

In 1971 Mercer and Dumas studied the composition of Ruthenium Blue synthesized via electrochemical reduction of potassium ruthenium chloride[16]. They reported that their Ruthenium Blue contains a series of $[Ru_2Cl_3]^{+2,3}$, $[Ru_2Cl_4]^{+1,2}$ and $[Ru_2Cl_5]^{0,+}$ species with the ruthenium atoms existing in various oxidation states. This was determined through potentiometric titrations, UV/Vis and ESR spectroscopic studies and electrochemical oxidations. No conclusive structure was given in the study, but it was proposed that a possible species in the Ruthenium Blue solution was a “tri-μ-chloro bridged ruthenium complex in octahedral configuration with aqua ligands filling the remaining coordination sites”.

The last notable study performed on the composition of Ruthenium Blue was carried out in 1980 by Bino and Cotton[18]. The authors proposed that Ruthenium Blue was composed of a $[Ru_3Cl_{12}]^{-4}$ species. This was inferred from x-ray crystallographic data of a blue precipitate that formed when adding $(C_2H_5)_4NCl$ to a solution of Ruthenium Blue. While an x-ray crystal was solved from the solution of Ruthenium Blue, the study concluded saying that the $[Ru_3Cl_{12}]^{-4}$ structure was not the final conclusion on the composition of Ruthenium Blue. The structure of the $[Ru_3Cl_{12}]^{-4}$ species is see in *Figure 5*.

Figure 5 – Structure of $[Ru_3Cl_{12}]^{-4}$ cluster by Bino and Cotton (1980)

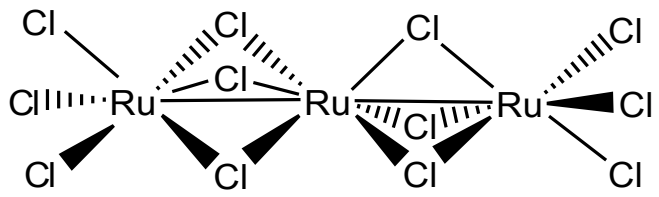

Obviously these studies do not agree on the composition of Ruthenium Blue. From the experiments presented in this thesis, it is thought that the species present in the negative-mode MALDI-ToF-MS of the blue compound are another possibility in identifying the species that make up Ruthenium Blue. The higher stability of the chemical species in the blue compound as compared to a solution of Ruthenium Blue is thought to arise from the reducing character of D-(+)-Glucosamine.

1.5 The CIE1931 Colour Metric

Human physiological interpretation of any sort of stimuli is inherently difficult to measure and quantify. The International Commission on Illumination (CIE) is the international body that standardizes the field of colorimetry and provides mathematical methods for interpreting and understanding the science of colour[19]. One of the first standard metrics of the physical interpretation of colour was developed in 1931 known as the CIE1931 XYZ Colour Space. This colour space was derived from a series of experiments performed by J. Guild[20].

Human vision is perceived through photoreceptors known as cone cells, of which we have three specific kinds that have peak sensitivities in specific areas of the visible spectrum. One set of cone cells detect light primarily in the blue region of the visible spectrum with the other sets detecting primarily in the green and red regions[21]. There is no set specific detection range of colour that is universal across humans since colour sensation is highly dependent on physical factors both directly and indirectly related to the eye of the observer. Since human eyes can only physically see the three primary colours of blue, green and red (from which colour addition processing from the brain makes up the rest of the colours), only three colour metrics are needed for mathematically determining colour perception[21].

Experiments were performed in order to determine the required amount of stimulus for each set cone cells in order to perceive a specific wavelength of light. Experiments by Guild involved setting up an observer at a station that showed light from a monochromator and from a tricolour red-blue-green source. At this station an operator would select light from a monochromator and the test subject would match the colour from the red-blue-green tricolour source by adjusting the brightness of the individual colours. Colours were matched in 5 nm increments starting from 780 nm and ending at 380 nm. What was seen from this experiment was that a specific brightness of the individual red-blue-green colours was used to generate the specific colour response across the visual spectrum.

This metric became known as the 1931 CIE Standard Observer RGB Colour Matching Functions. These RGB Colour Matching Functions can be see in *Figure 6*.

Figure 6 – The 1931 CIE Standard Observer RGB Colour Matching Functions

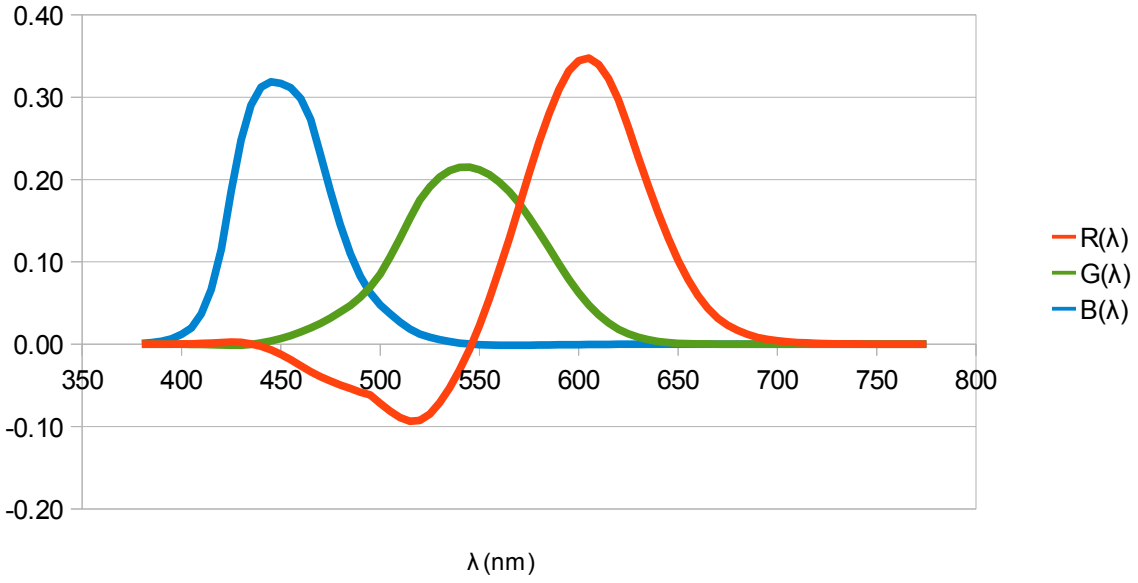

While these RGB Colour Matching Functions were sufficient in describing the stimulus needed for reproducing a particular colour standard using a tricolour experimental colour, limitations for universal theoretical use still existed. The individual Colour Matching Functions needed to be normalized with each other. Additionally elimination of the negative regions of the Colour Matching Function, an artifact from needing to add a portion of particular colour to the standard test colour as opposed to the experimental colour, was needed as negative numbers

were difficult to process during the time of development. As a result a matrix transformation for the functions to be useful was experimentally determined. The matrix is seen in *Figure 7.*

Figure 7 – Matrix Transformation to Convert the CIE1931 RGB Colour Matching Functions into the CIE1931 XYZ Colour Matching Functions

$$\begin{vmatrix} X \\ Y \\ Z \end{vmatrix} = \begin{vmatrix} 2.768892 & 1.751748 & 1.130160 \\ 1.000000 & 4.590700 & 0.060100 \\ 0 & 0.056508 & 5.594292 \end{vmatrix} \cdot \begin{vmatrix} R \\ G \\ B \end{vmatrix}$$

Thus this matrix conversion allows for the Colour Matching Functions to be of isoenergetic in their intensities and elimination of the negative portion of the Colour Matching Functions. The resulting Colour Matching Functions, the CIE1931 XYZ Colour Matching Functions are seen in *Figure 8*.

Figure 8 – The 1931 CIE Standard Observer XYZ Colour Matching Functions

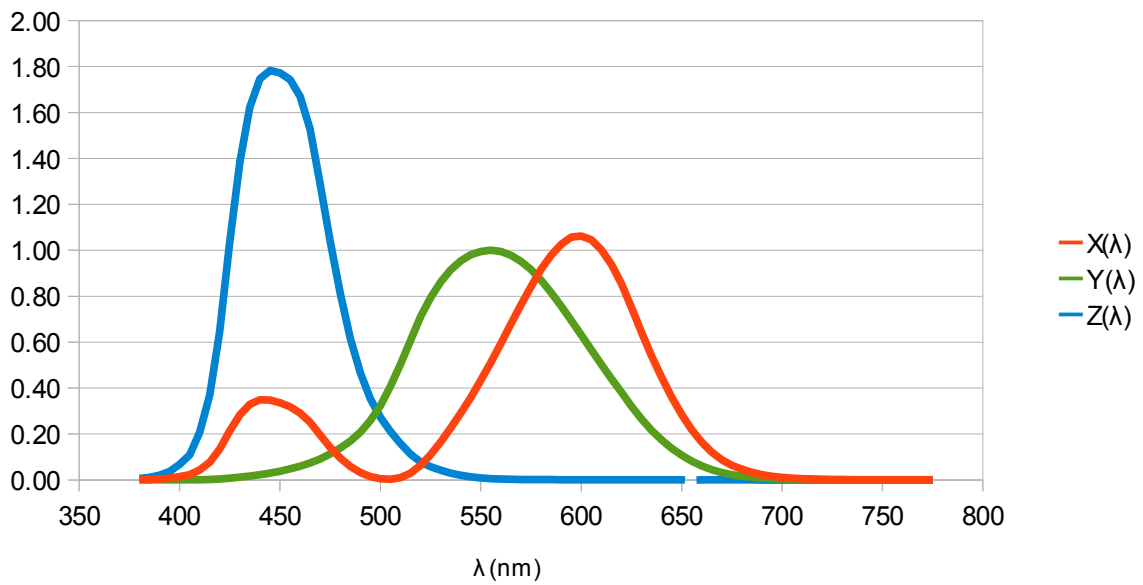

The creation of the CIE1931 Colour Space and resulting metric involved development and refinement that spans across the late 19th century to the early 20th century involving work from the fields of mathematics and optics. The theory behind the CIE1931 Colour Space, seen in *Figure 9*, is beyond the scope of this thesis and is not described here.

Figure 9 – The CIE1931 Colour Space[19]

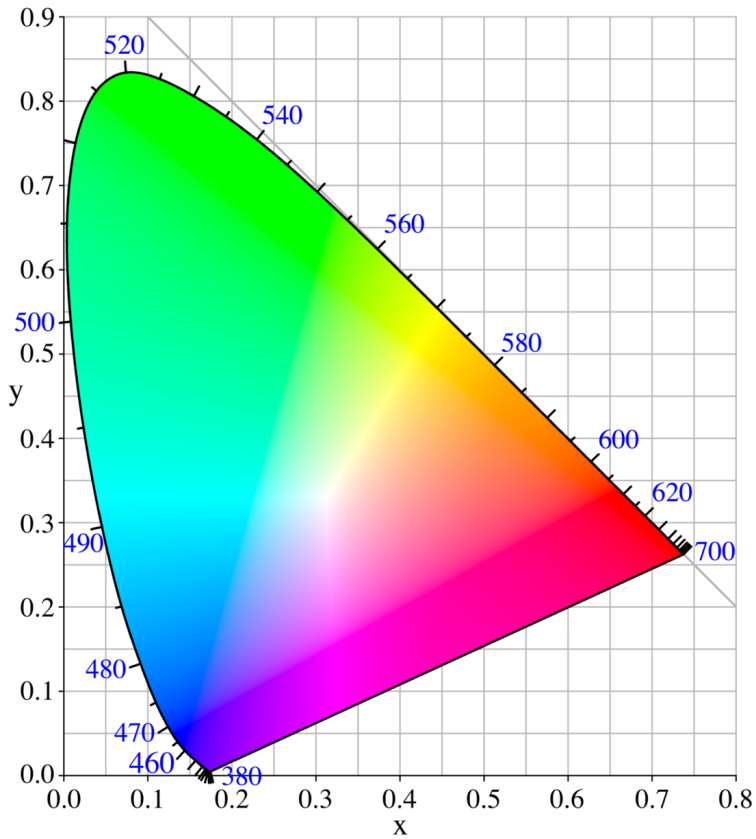

1.6 Overview of Research Project

It has been reported previously in the literature that the colour perception of various organic chemical indicators can be determined from their experimental UV/Vis absorption spectra. Work done by Mortimer and Varley showed that the UV/Vis spectra of these organic indicators could be plotted on the International Commission on Illumination CIE1931 colour space from experimental data

obtained from a spectrophotometer[22]. By using the International Commission on Illumination mathematical methods for interpreting colour, Mortimer and Varley showed that using a simple spreadsheet program, a UV/Vis spectra as a series of data points can be processed to the respective colour space coordinates and thus plotted on CIE1931 colour space in order to determine the perceived colour.

From a more theoretical study, Beck showed that the physically perceived colour of 8 of 9 dyes could be successfully predicted from TD-DFT generated electronic excitation spectra using a Becke-Perdew combination of functionals and a TZVP basis set[23]. The single unsuccessful outlier was Malachite Green where the 0→1 and 0→2 transitions were blue and red-shifted respectively. The work done by these researchers showed that the ability to successfully predict the physically perceived colour of organic compounds is possible both experimentally and theoretically from *ab initio* calculations. Thus it was envisioned that this method of converting a UV/Vis spectra into CIE1931 colour space coordinates could also be applied to electronic excitation calculations of the ruthenium chloride clusters.

The purpose of the work described in this thesis is to determine the chemical formula of the species present in the MALDI-ToF-MS negative mode spectrum of the product formed from boiling $RuCl_3 \cdot 3H_2O$ and D-(+)-Glucosamine in ethanol. On the identified species, *ab initio* calculations are performed to

determine the molecular geometry and electronic excitation spectra in order to predict the visible colour change as the product degrades from blue to green to yellow.

Chapter 2: Experimental

2.1 Synthetic Methods

In order to coordinate D-(+)-Glucosamine to a ruthenium centre, a good ruthenium precursor was needed. This precursor needed be readily accessable, highly robust for coordination and low solvent toxicity. Ruthenium Blue fits these characteristics and was used as the coordination precursor of choice. The synthesis of Ruthenium Blue was taken from the work published by Togano et al. [17] The procedure called for refluxing $RuCl_3 \cdot 3H_2O$ with ethanol under an inert atmosphere for approximately 5-6 hours. Completion of the reaction is indicated when the solution changes from yellow/brown to green and finally a notably vibrant blue.

2.2 Computational Methods

As with all computational studies, the decision of the basis set and method used for the calculations a comprimise between computational time and basis set accuracy. A “first-pass” optimization of the rationally designed input structures was performed using the Slater-type Orbital basis set of STO-3G in order to refine the structures for higher level calculations[24]. Slater-type orbitals are notorious for being highly inaccurate in proper modelling of the molecular orbitals of a chemical species. Hence normal termination was occasionally difficult to achieve, either through convergence failures of the Self-Consistant Field steps of

the calculations or through the optimization procedure being unable to find a stationary point. In these cases energy shifting of the molecular orbitals through the keyword “scf=vshift” or lowering the points per atom of the integral grid using the keyword “Int=(CoarseGrid)”.

As Slater-type orbitals are unacceptably inaccurate for publication a higher level of theory is needed for accurate results. A combination basis set was employed to use effective core potentials (ECP) on the ruthenium atoms, while using a non-ECP basis set on the chlorine atoms. The doublet-zeta Stuttgart/Dresden (SDD)[25] basis set was used for the ruthenium atoms while a Pople basis set of 6-311G(2d)[26] was used on the chlorine atoms. As the colours were determined as a solution, it was necessary to include solvent effects for the calculations. All calculations were performed using a Polarizable Continuum Model (PCM)[27] in order to reproduce this while the solvent model used was water. While using water may seem unusual as the Ruthenium Blue already is present in a solvent of ethanol, samples used for colour determination had the ethanol stripped and replaced with water so that the solution would not dry out within hours.

The method of choice for calculating the geometry and electronic excitations of the clusters was Density Functional Theory (DFT). DFT was chosen over other methods such as Møller–Plesset perturbation theory for

geometry optimizations or CCS(D) and CIS for the electronic excitations due to previously seen investigations into geometry optimization and electronic excitations using DFT and Time-Dependent DFT (TDDFT) for transition metal species. Also the uniformity of using Density Functional Theory for all calculations of the study of the ruthenium chloride clusters was considered necessary.

GaussView5 is not capable of making reliable predictions for the bonding of the optimized ruthenium chloride clusters. As a result bonding information was obtained from the molecular orbital overlap information from the output file of the optimization. The program AOMix developed by Gorelski[28],[29] was used to determine the proper bonding of the clusters using Natural Bonding Overlap (NBO) analysis.

2.3 Synthesis of the Blue Compound

The synthesis of the blue compound was performed by reacting 50 mg of D-(+)-Glucosamine with 1 equivalent of $RuCl_3 \cdot 3H_2O$ *(calc. 73mg).* Using 95% ethanol as a solvent and under an inert atmosphere of argon, the solution of glucosamine and ruthenium was heated to reflux for 12 hours. The solvent was evapourated off affording a deep blue solid. $RuCl_3 \cdot 3H_2O$ was obtained from Pressure Chemicals and D-(+)-Glucosamine was obtained from Sigma-Aldrich.

2.4 *Ab initio* calculations on Ruthenium Chloride clusters

All *ab initio* calculations were performed using Gaussian09 Rev. A.02[30]. Calculations were performed using the Density Functional Theory method with the PBE0 functional and a combination basis set of SDD for Ru atoms and 6-311G(2d) for Cl atoms. Vibrational frequency analysis was performed on all optimizations to ensure a true ground state geometry was obtained. TD-DFT calculations were performed to obtain the electronic excitation energies of all reported clusters. Stability tests were performed on all clusters to ensure ground electronic state was used for input into TD-DFT calculations. Geometry optimizations, frequency and TD-DFT calculations were performed with a Polarizable Continuum Model solvent system for water.

2.5 Processing of Electronic Excitations into UV/Vis spectra

UV/Vis spectra of the clusters were generated using a Half-Width, Half-Height of 0.305 eV. CIE1931 (*x,y*) chromacity coordinates were generated using the program *Calc* from the *OpenOffice* suite of programs[31]. The methodology for the generation of the CIE1931 colour space chromacity coordinates for the clusters is shown in *Figure 10*.

Figure 10 – Flowchart of the methodology for calculating the perceived physical colour of the ruthenium chloride clusters

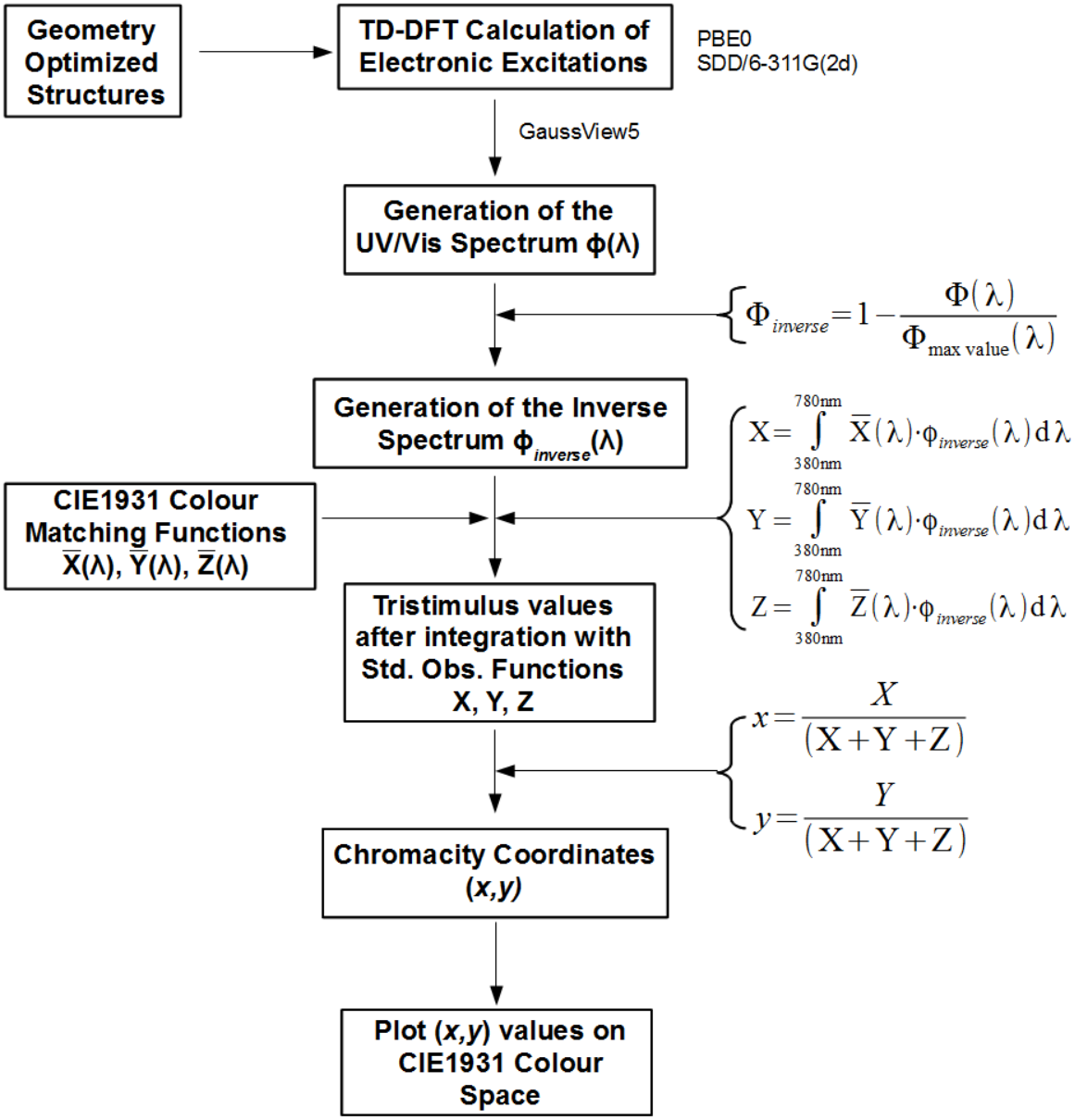

A walkthrough of *Figure 10* is as follows: TD-DFT calculations of the geometry optimized clusters were performed to enough excited states to ensure that electronic excitations to at least 300 nm were obtained. The CIE1931 colour matching functions range from 780 to 380 nm, thus calculating UV/Vis spectra to 300 nm would provide a complete UV/Vis spectra of the cluster.

The next step in the conversion involves inversion of the calculated excitation spectra and normalization to 1. This is inversion/normalization is depicted in *Figure 11*.

Figure 11 – Example of Inversion and normalization of electronic excitation spectra using the spectrum of $[Ru_2Cl_6]^-$

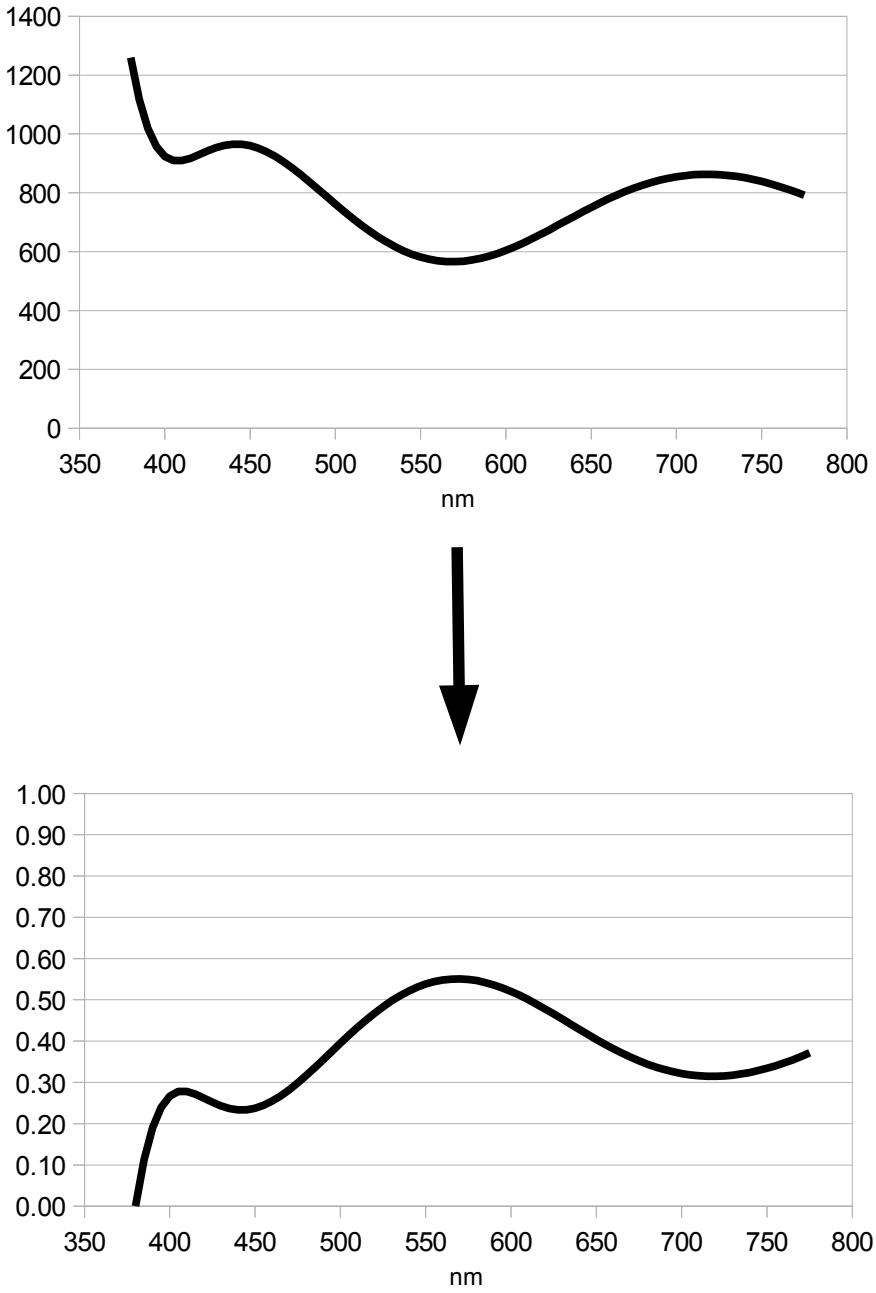

As stated before this inversion can be performed by any standard spreadsheet program. The UV/Vis spectrum is entered into the spreadsheet as a series of *X*-*Y* points, with *X* being the wavelength and *Y* being the absorbance. To invert the *Y* values, the following conversion factor is applied see in *Figure 12*.

Figure 12 – Conversion Function for Inversion of the UV/Vis spectrum

$$f(x) = 1 - \frac{(Experimental\ Absorbance)}{(Maximum\ Absorbance\ Value)}$$

In order to determine the maximum absorbance value, *OpenOffice* contains a specific function that can determine the maximum value in a series of data points. The specific code for this function for entry into a spreadsheet cell can be seen in *Figure 13.*

Figure 13 – Code for Determining the Maximum Value of a Series of Data Points

```
=MAX(range1:range2)
```

At this stage the *X*-*Y* coordinates of the inverted spectrum are obtained. The inverse spectra is then integrated with each of the CIE1931 Colour Matching functions from 380 to 780 nm to create the CIE1931 Tristimulus Values of Red, Blue and Green. The CIE1931 Colour Matching functions are shown in *Figure 14*.

Figure 14 – CIE1931 Colour Matching Functions

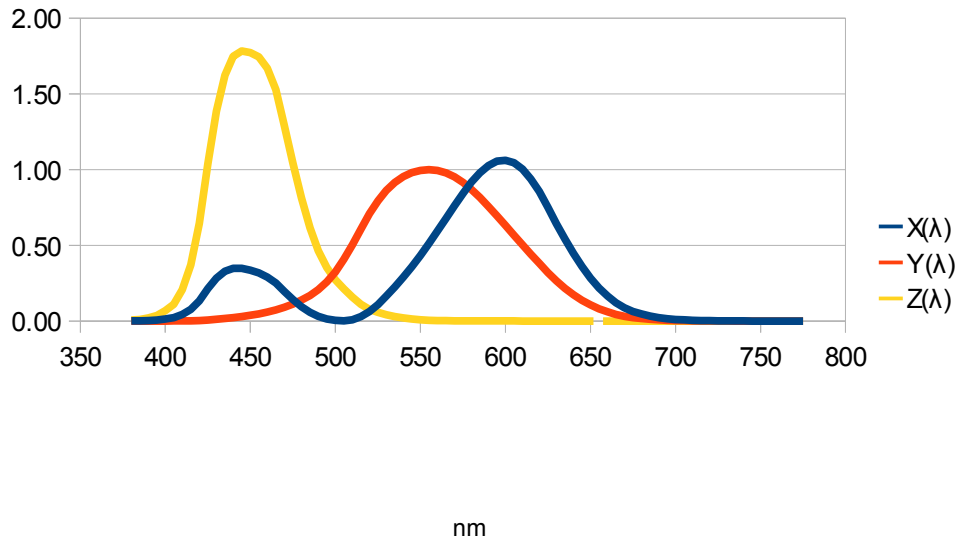

The mathematical equation for integrating the inverted UV/Vis spectrum with the CIE1931 Colour Matching Functions to obtain the Tristimulus values was taken from Beck's study of TD-DFT generated absorption spectra of organic dyes. The functional is shown in *Figure 15.*

Figure 15 – Functional for Obtaining the Tristimulus Values from Integration of the Inverted Absorption Spectrum with the CIE1931 Colour Matching Functions from Beck[23]

$$X = \int_{400\,nm}^{700\,nm} d\lambda\, X(\lambda) \cdot \text{inverse\_spectrum}\left(\frac{hc}{\lambda}\right)$$

Breaking down this equation we can see that obtaining the tristimulus value is just a series of multiplication steps finished by a summation. These steps are broken down as a series of steps as follows:

1. Multiplying each individual point by the respective point on the colour matching function
2. Multiplying the product from Step 1 by the change in wavelength between the points, in this study the value is 5 nm
3. Summing the product of Step 2 across the entire spectrum, in this study the wavelengths considered were between 780 nm and 380 nm.

At this stage we now have the three Tristimulus values of X, Y and Z. The Tristimulus values are then summed and normalized into the Chromacity Coordinates where the X and Y values are used (Z is omitted). Normalization can be performed using the function shown in *Figure 16.*

Figure 16 – Normalization function of the Tristimulus Values into Chromacity Coordinates for *x* and *y* respectively

$$x = \frac{X}{(X+Y+Z)} \qquad y = \frac{Y}{(X+Y+Z)}$$

These points are then plotted on the CIE1931 Colour Space metric, shown in *Figure 17*, which show the physically interpreted colour.

Figure 17 – CIE1931 Colour Space Metric

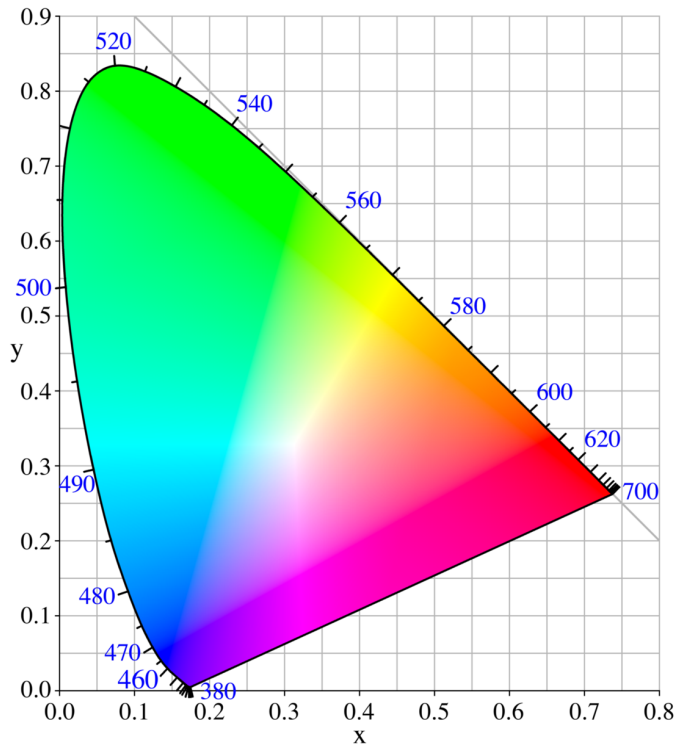

Overlapping of the UV/Vis spectra of the various ruthenium chloride clusters to generate the a combined spectrum of the specific Blue, Green and Yellow solutions were simply made by determining the maximum absorbance of each wavelength and using that value for the combined spectrum. This was achieved using the =MAX(range1:range2) function seen previously in *Figure 13*.

2.6 Methods for Mass spectrometry of Ruthenium Chloride clusters

For MALDI-ToF-MS, $RuCl_3 \cdot 3H_2O$ was mixed directly with a matrix solution composed of 2 mg of 3,4-dihydroxy-benzoic acid in 20% of ethanol. An analyte–matrix 1:2 ratio (*v*/*v*) and 1 mL was spotted on the MALDI sample target and allowed

to dry at room temperature. For LDI-ToF-MS, a few crystals of analyte were deposited on the sample target and gently pressed toward the target. The analyses were per- formed using a MALDI-ToF-MS instrument (model Reflex III, Bruker) equipped with a 337 nm nitrogen laser. Samples were analyzed in reflectron and negative ion modes. Ion sources 1 and 2 were held at 20 and 16.35 kV, respectively. The guiding lens voltage was set at 9.75 kV. The reflector detection gain was set at 5.3 with pulsed ion extraction at 200 ns. The nitrogen laser power was set to the minimum level necessary to generate a reasonable signal and avoid possible degradation of analytes. Typically, 15% of laser energy was used, which was calculated to be 4 mJ. In the case of high laser energy experiments, 45% of laser energy was used, which equalled 12.5 mJ. The pulse duration was 9 Hz, the spot size was 2 mm, and the calculated energy density was 100 μJ / 0.1mm^2. A two-point external calibration was performed, using the $[M – H]^–$ (153.01 Da) and $[2M – H]^{–2}$ (447.12 Da) peaks of dehydroxybenzoic acid and the dimer of sinapinic acid, respectively, prepared in acetonitrile–water solution (10 pmol/mL).

Chapter 3: Results and Discussion

3.1 Ruthenium Blue Compound

Over the 12 hours of refluxing glucosamine and ruthenium chloride, the solution progressed from the original yellow/brown colour to a green colour and lastly that of the final vibrant blue. The first colour change from yellow/brown to green becomes apparent after approximately 90 minutes of refluxing. However the second colour change of green to blue takes much longer and occurs between 10 to 12 hours from start of refluxing. The blue compound is moderately air and water stable. However when kept in solution and exposed to the ambient atmosphere, the blue colour fades to green within 3 to 4 days followed by a change from green to yellow/brown after an additional 4 to 6 days. *Figure 18* shows solutions of the blue compound at the various stages of decomposition. IR spectroscopy of the blue compound showed no evidence of remaining glucosamine while NMR experiments showed no evidence of any compound in the sample, typical of a sample containing paramagnetic species. Additionally the blue compound dissolves only in polar solvents.

Figure 18 – Solutions of the blue compound at various stages of decomposition. a) blue, b) green c) yellow

a) **b)** **c)**

3.1.1 <u>Mass Spectrometry results of Blue Compound</u>

MALDI-ToF-MS experiments with the blue compound, seen in *Figure 20*, show that coordination of glucosamine to ruthenium was not achieved as there was no peak difference indicative of a 178 *m/z* glucosamine fragment. What was seen from the mass spectrum was a series of peaks between 0 and 1000 *m/z* matching the isotopic pattern of various ruthenium chloride species. Only spectra in the negative mode showed showed any sensible peaks indicative of ruthenium chloride clusters. The peaks seen in the mass spectrum of the blue compound matches that of the LDI-ToF-MS spectrum of the starting material $RuCl_3 \cdot 3H_2O$ in terms of *m/z*, however the relative abundances of the peaks between the two spectra differ. As well, the LDI-ToF-MS spectrum of $RuCl_3 \cdot 3H_2O$ shows a substantial peak at 35 *m/z* indicative of a chlorine atom. The LDI-ToF-MS of $RuCl_3 \cdot 3H_2O$ is shown in *Figure 19*[32].

Figure 19 – LDI-ToF-MS of $RuCl_3 \cdot 3H_2O$[32]

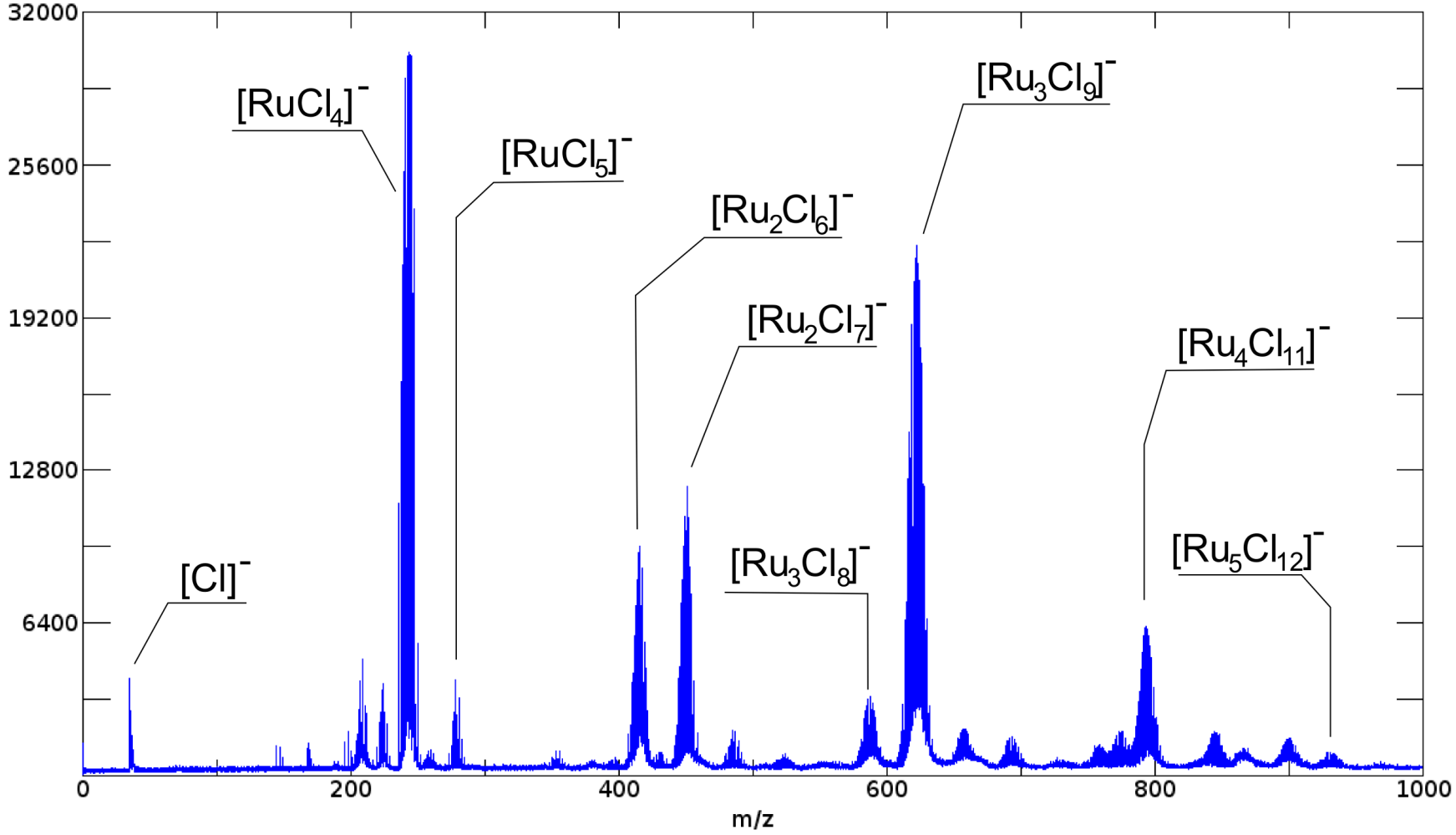

However this peak at 35 *m/z* is absent in the MALDI-ToF-MS of the Blue Compound. It has been established that the ruthenium chloride clusters that were detected from the LDI-ToF-MS spectrum of $RuCl_3 \cdot 3H_2O$ were generated by the laser desorption ionization (LDI) process, a phenomena that has been reported for many transition metal elements with various coordinated ligands. However it does not seem that the ruthenium chloride clusters detected in the blue compound were generated via LDI. The three spectra in *Figure 20-22* show a gradual reduction from the larger ruthenium chloride clusters to the smallest as the product degrades. If the clusters were generated from the LDI process of the analysis, then the same number and relative abundance of the ruthenium chloride clusters would be seen across the three spectra. Since this does not occur, it is concluded that the ruthenium chloride clusters from the Blue Compound are generated in solution and not from the LDI process.

Figure 20 – MALDI-ToF-MS spectra of the Blue Compound at the blue degradation stage. Negative mode

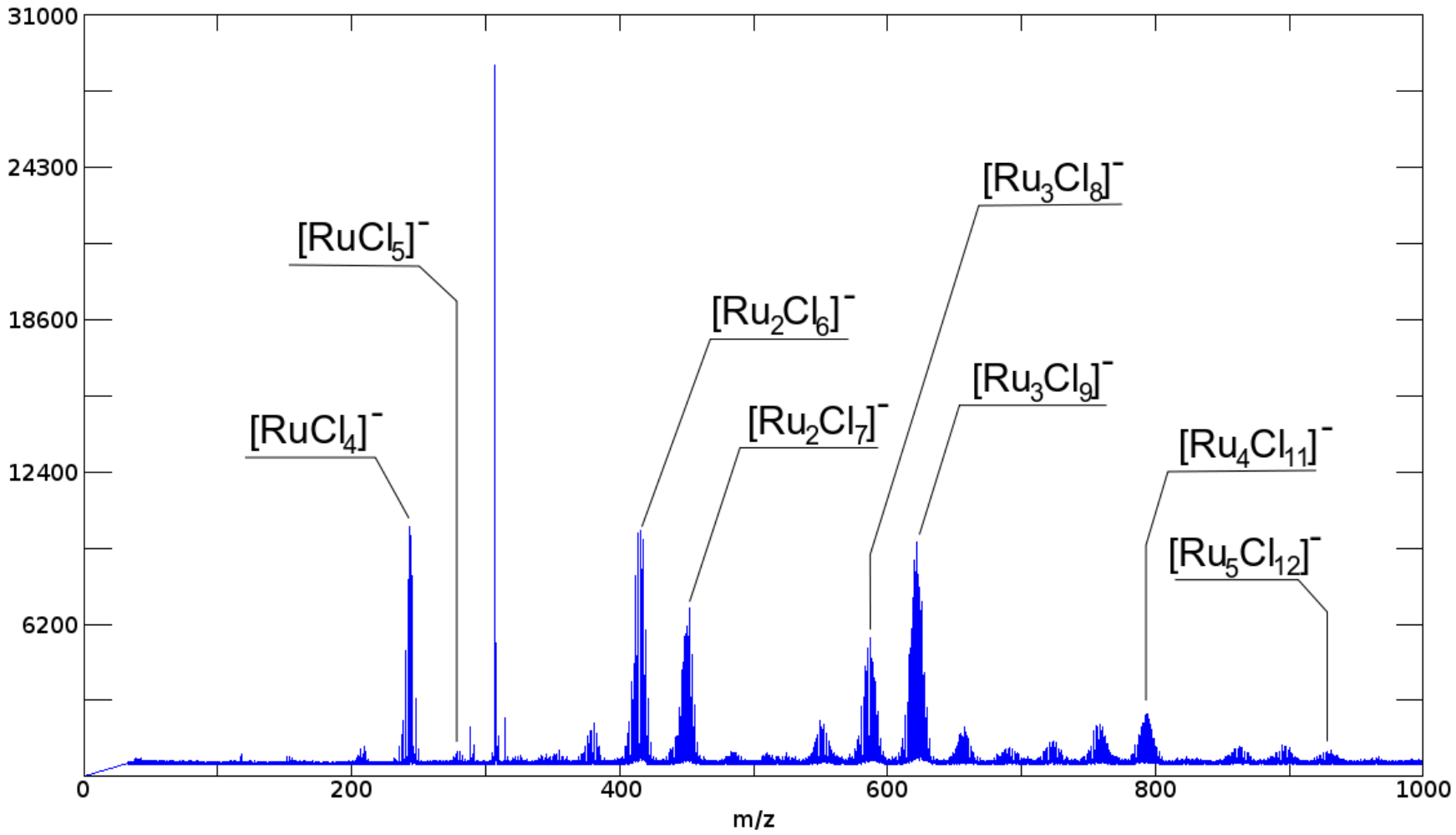

Figure 21 – MALDI-ToF-MS spectra of the Blue Compound at the green degradation stage. Negative mode

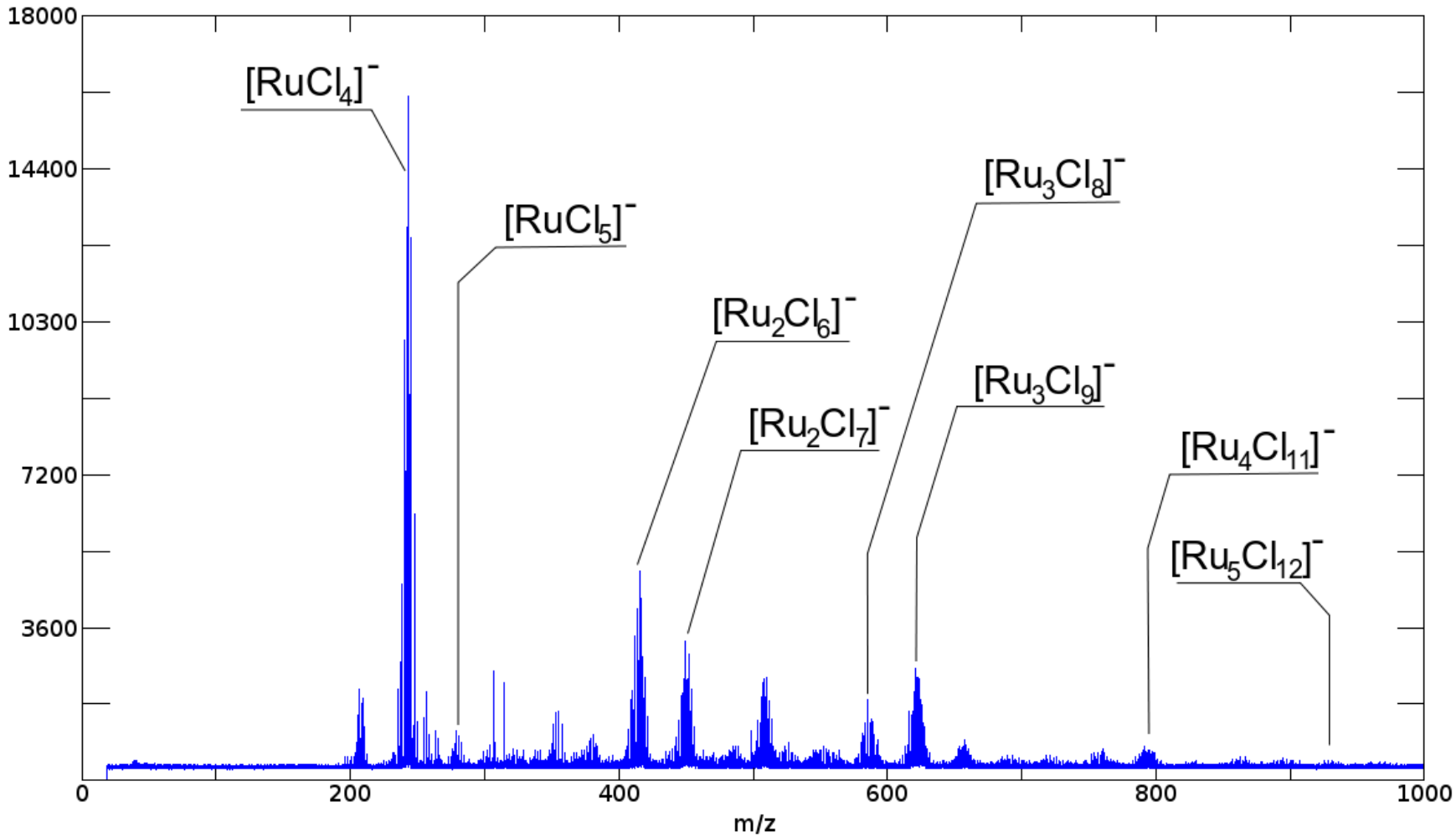

Figure 22 – MALDI-ToF-MS spectra of the Blue Compound at the yellow degradation stage. Negative mode

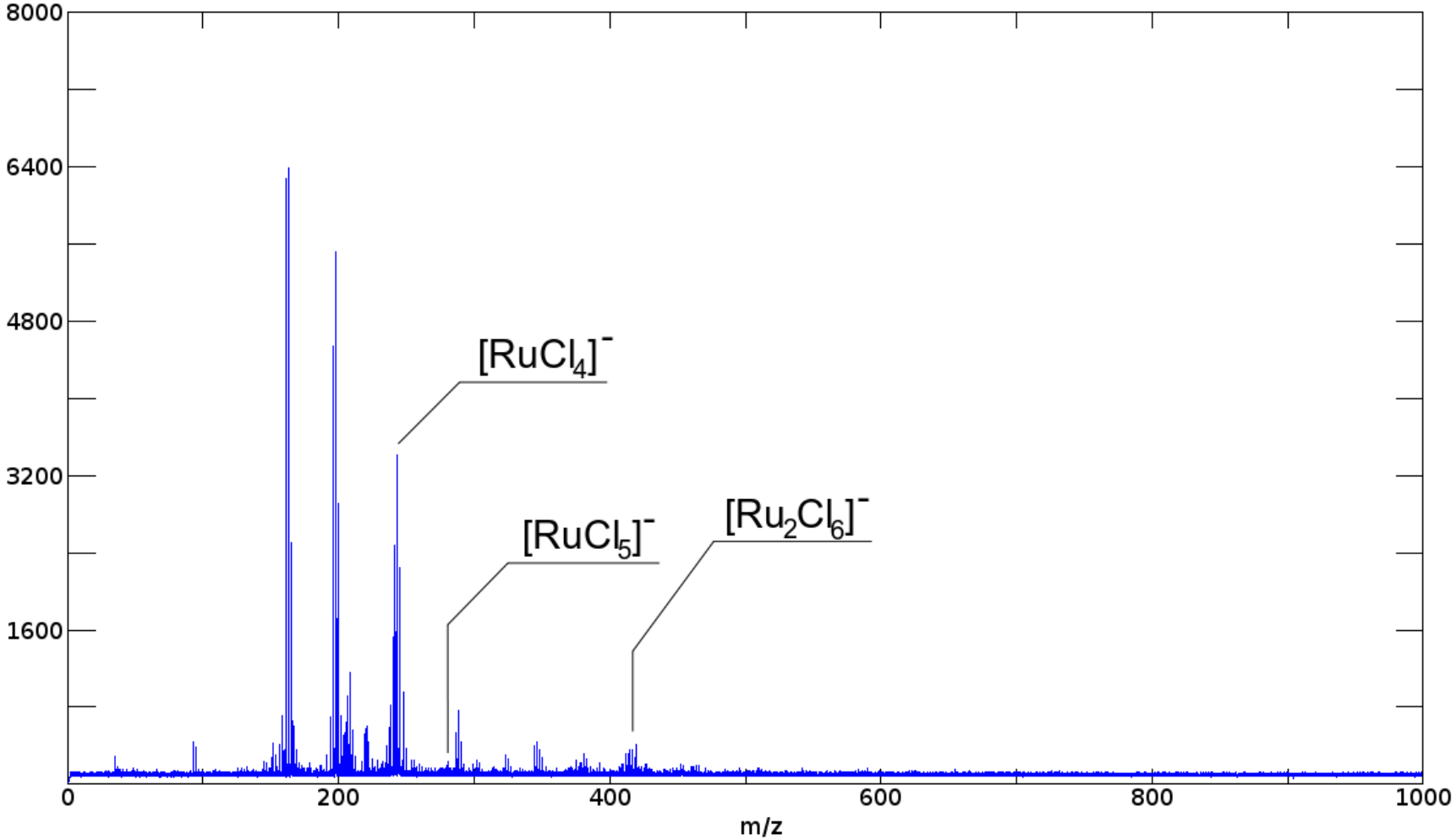

3.2 *Ab initio* results on Ruthenium Chloride clusters

To obtain structures for the ruthenium chloride clusters as input for DFT calculations, chemical formulas of the individual peaks were determined using the isotope profile. Since ruthenium has 7 stable isotopes, any ruthenium containing species can be identified through its unique isotopic profile. The process of identifying the ruthenium chloride clusters in the the MALDI-ToF-MS spectrum started by making a list of all the possible ruthenium chloride combinations from 0 to 1000 g/mol with the assumption that ruthenium has a maximum coodination number of six and multi-ruthenium species are present. From this list the masses of the formulas were calculated and matched against the *m/z* of the peaks present in the spectrum. Of those matched species, computed isotopic profiles were generated and compared to the profile of the experimental peak to determine if there is a match. With this method, only one ruthenium chloride species can be considered a match against the peaks of the experimental spectrum. An example of this comparison of the computed isotopic profile (in orange) is seen against the experimental MALDI-ToF-MS spectrum (in blue) for the clusters $[Ru_2Cl_6]^-$ and $[Ru_3Cl_9]^-$ in *Figure 23* and *Figure 24* respectively.

Figure 23 – Experimental (top,blue) and Calculated (bottom, orange) Mass Spectrum Profile of $[Ru_2Cl_6]^-$

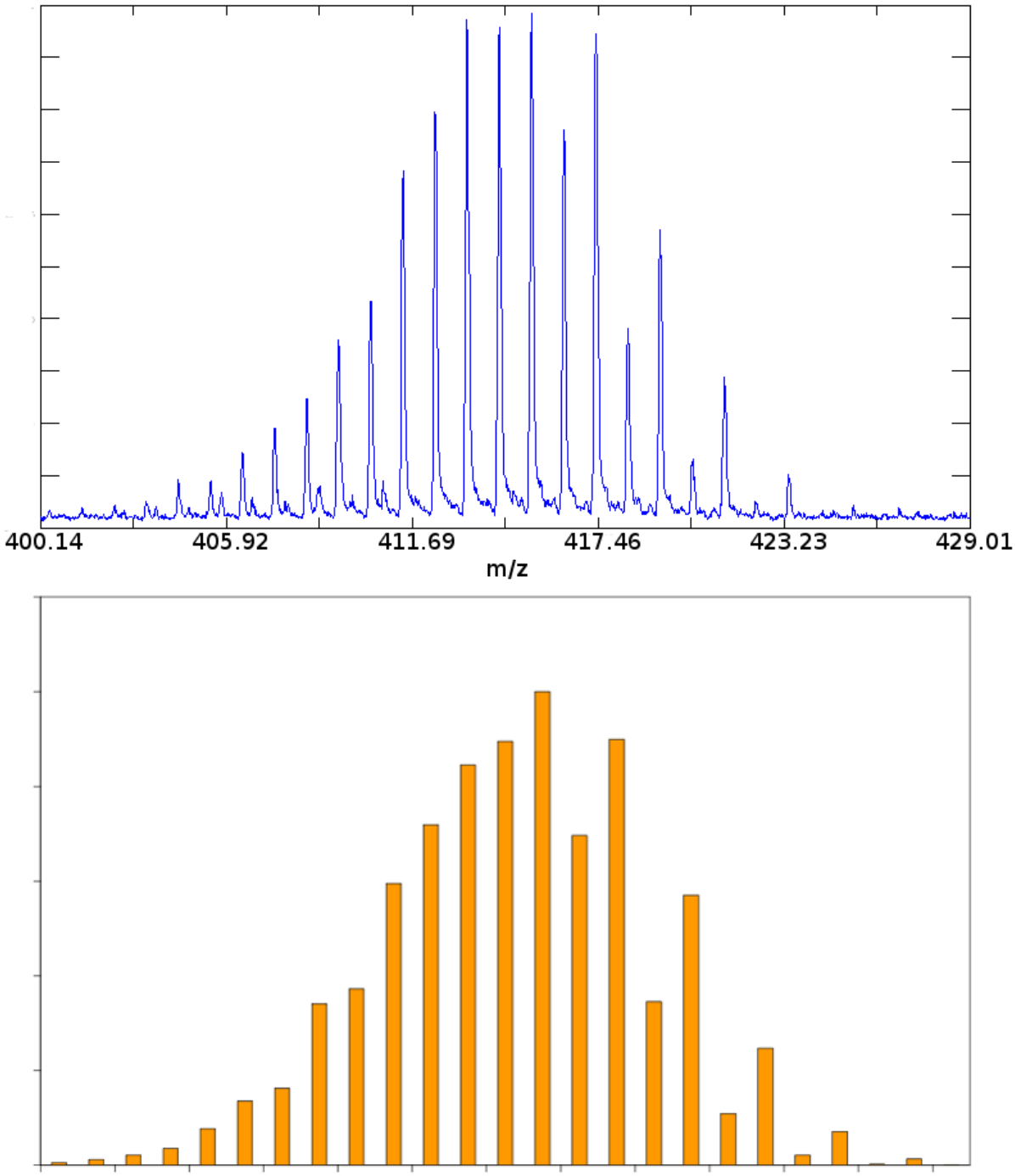

Figure 24 – Experimental (top,blue) and Calculated (bottom, orange) Mass Spectrum Profile of $[Ru_3Cl_9]^-$

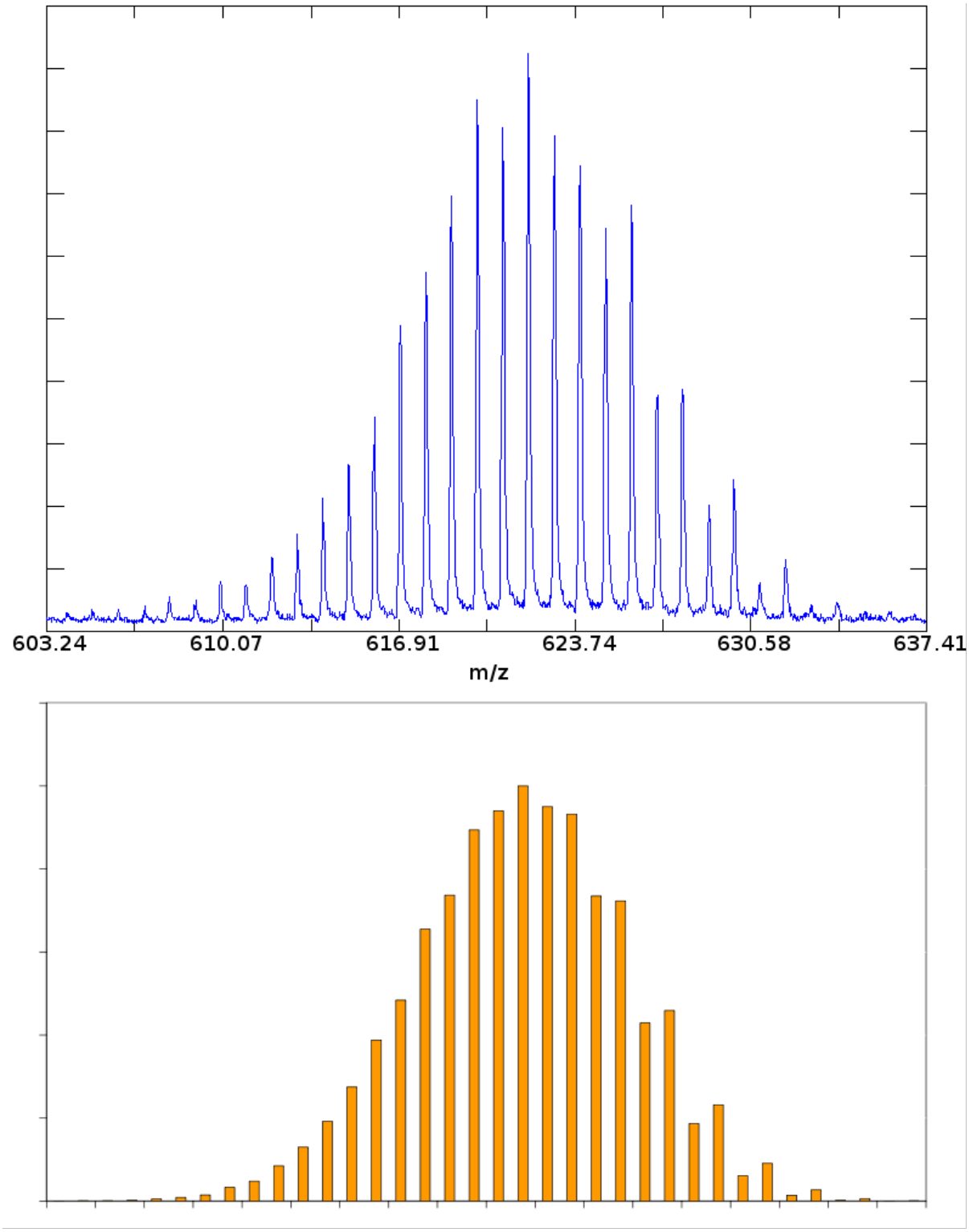

At this point input geometries for the *ab initio* calculations were rationally designed and drafted from the matched chemical formulas based on sensible structures that contained Ru-Cl-Ru and Ru-Ru bonds. The optimized structures were verified as minimized by vibrational analysis to ensure no imaginary vibrational frequencies existed and by testing the wavefunction stability to ensure that the geometry and multiplicity was that of the ground electronic state. Stability tests of the ruthenium chloride clusters showed that the singlet and doublet multiplicities were seldom the ground electronic state and higher multiplicities had to be used in order to obtain the true ground state. *Figure 25* shows the output of the *ab initio* calculations and the resulting final geometry of the ruthenium chloride clusters.

Figure 25 – Structures of the Ruthenium Chloride Clusters

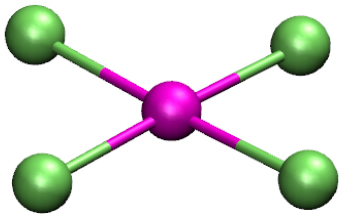

$[RuCl_4]^-$

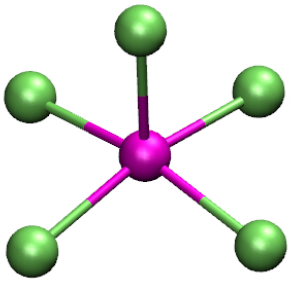

$[RuCl_5]^-$

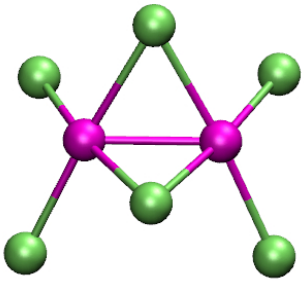

$[Ru_2Cl_6]^-$

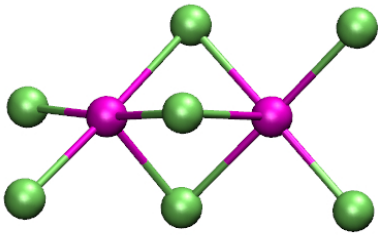

$[Ru_2Cl_7]^-$

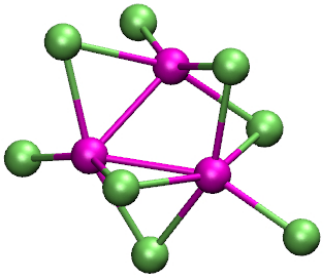

$[Ru_3Cl_8]^-$

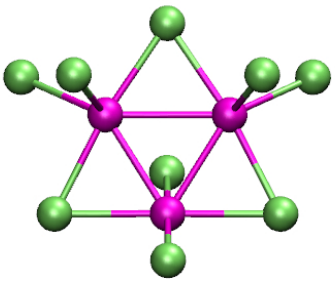

$[Ru_3Cl_9]^-$

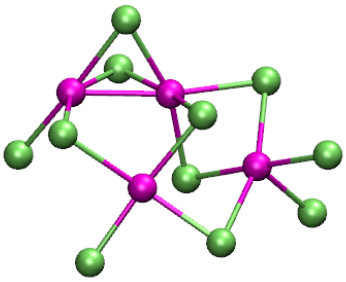

$[Ru_4Cl_{11}]^-$

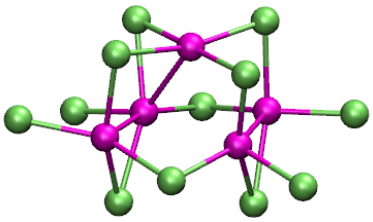

$[Ru_5Cl_{12}]^-$

As described above, the blue compound that was generated degrades in solution in a signature fashion, turning from it's vibrant blue to green and finally to yellow/brown. Addtionally, MALDI-ToF-MS spectra were taken of the blue compound at it's various stages of decomposition in order to determine what the chemical make up at each stage was and they are seen in *Figure 20-22*. We used the “blue solution” MALDI spectrum as a reference standard with no decomposition occurring. Comparison with the spectra of the “green solution” shows that there is a sharp decrease in the abundance of $[Ru_5Cl_{12}]^-$, $[Ru_4Cl_{11}]^-$, $[Ru_3Cl_9]^-$ and $[Ru_3Cl_8]^-$ with a sharp increase in the abundance of $[RuCl_4]^-$. The decomposition of a solution of the blue compound hence involves the breakdown of the larger ruthenium chloride clusters into $[RuCl_4]^-$. When comparing the spectra of the “blue solution” and “green solution” to that of the “yellow solution”, the only chemical species that are still present are $[RuCl_4]^-$, $[RuCl_5]^-$ and $[Ru_2Cl_6]^-$ with chemical species peaks that are present at 195 and 170 *m/z.* Attempts to identify these species using the isotope profile were unsuccessful as no match to that of a ruthenium chloride cluster could be found.

The presence of the ruthenium chloride cluster species present at each colour stage is tabulated in *Table 2*.

Table 2 – Composition of the Blue Compound at Various Colours

Colour	Clusters Evident
Blue	$[RuCl_4]^-$ --> $[Ru_5Cl_{12}]^-$
Green	$[RuCl_4]^-$ --> $[Ru_5Cl_{12}]^-$
Yellow	$[RuCl_4]^-$ --> $[Ru_2Cl_6]^-$

3.3 Calculated Electronic Excitation Spectra of Ruthenium Chloride Clusters

From the evidence presented by the MALDI-ToF-MS spectra of the blue compound showing the successive degradation of the ruthenium chloride clusters as the colour of the product changed, it was concluded that the colour of the compound was dependent on the combined absorption spectra of the individual ruthenium chloride species. Therefore by overlapping the proper combination of individual UV/Vis spectra of the ruthenium chloride clusters, it would be possible to show the colour change presented by the degradation of the blue compound. Thus UV/Vis spectra were generated for all of the reported ruthenium chloride clusters from the calculated electronic excitations. The spectra show that all clusters, except $[Ru_4Cl_{11}]^-$, absorb light in the blue/violet region which would be physically perceived as yellow. The outlier $[Ru_4Cl_{11}]^-$ strongly absorbs light in the orange region making it physically perceived as blue. The UV/Vis spectra of each of the reported clusters is see in *Figure 26*. The CIE1931 chromacity coordinates of the various solutions is seen in *Table 3* and their location in colour space is seen in *Figure 27*.

Figure 26 – UV/Vis spectra of Ruthenium Chloride Clusters. (a) $[RuCl_4]^-$, (b) $[RuCl_5]^-$, (c) $[Ru_2Cl_6]^-$, (d) $[Ru_2Cl_7]^-$, (e) $[Ru_3Cl_8]^-$, (f) $[Ru_3Cl_9]^-$, (g) $[Ru_4Cl_{11}]^-$, (h) $[Ru_5Cl_{12}]^-$

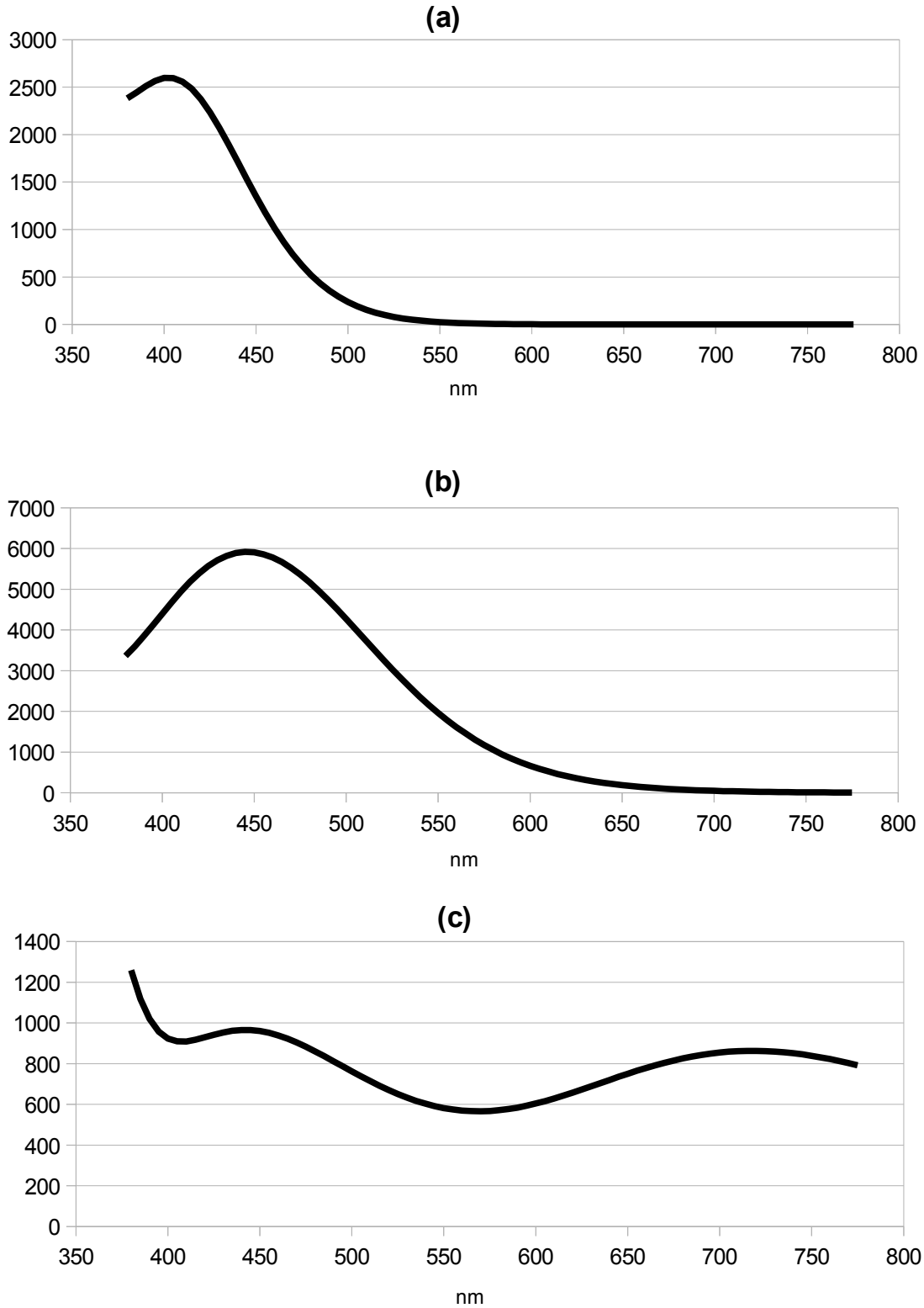

Figure 26 – UV/Vis spectra of Ruthenium Chloride Clusters. (a) $[RuCl_4]^-$, (b) $[RuCl_5]^-$, (c) $[Ru_2Cl_6]^-$, (d) $[Ru_2Cl_7]^-$, (e) $[Ru_3Cl_8]^-$, (f) $[Ru_3Cl_9]^-$, (g) $[Ru_4Cl_{11}]^-$, (h) $[Ru_5Cl_{12}]^-$

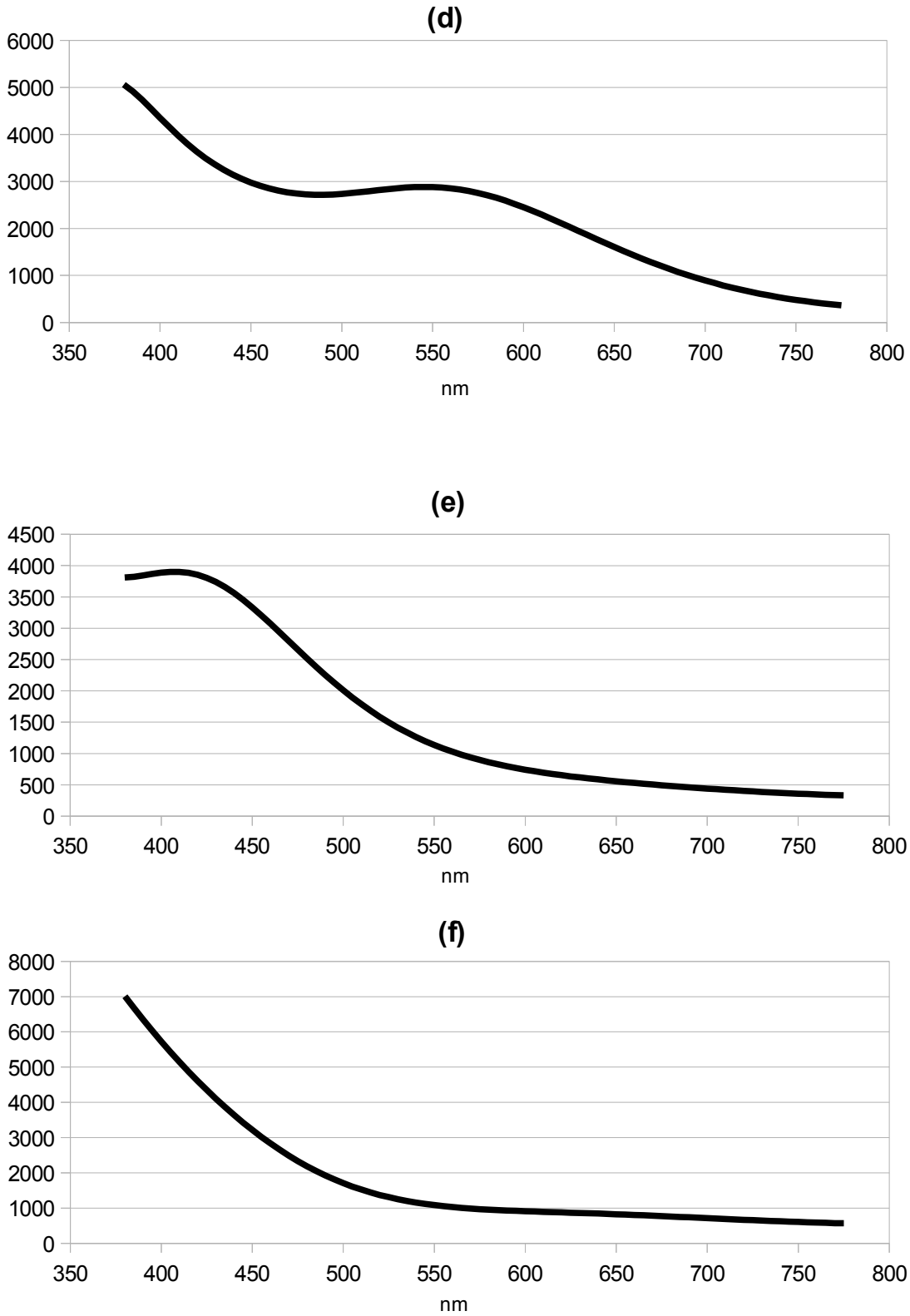

Figure 26 – UV/Vis spectra of Ruthenium Chloride Clusters. (a) $[RuCl_4]^-$, (b) $[RuCl_5]^-$, (c) $[Ru_2Cl_6]^-$, (d) $[Ru_2Cl_7]^-$, (e) $[Ru_3Cl_8]^-$, (f) $[Ru_3Cl_9]^-$, (g) $[Ru_4Cl_{11}]^-$, (h) $[Ru_5Cl_{12}]^-$

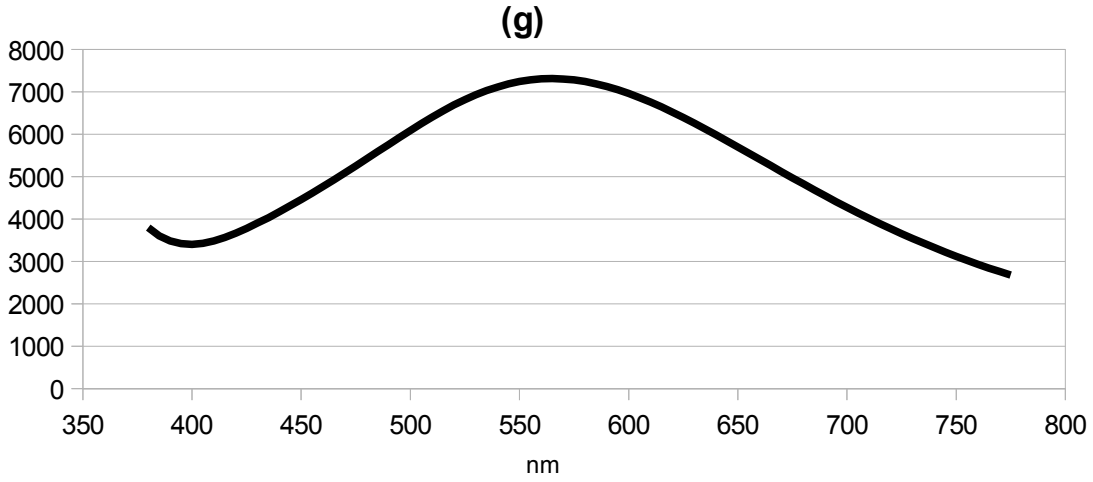

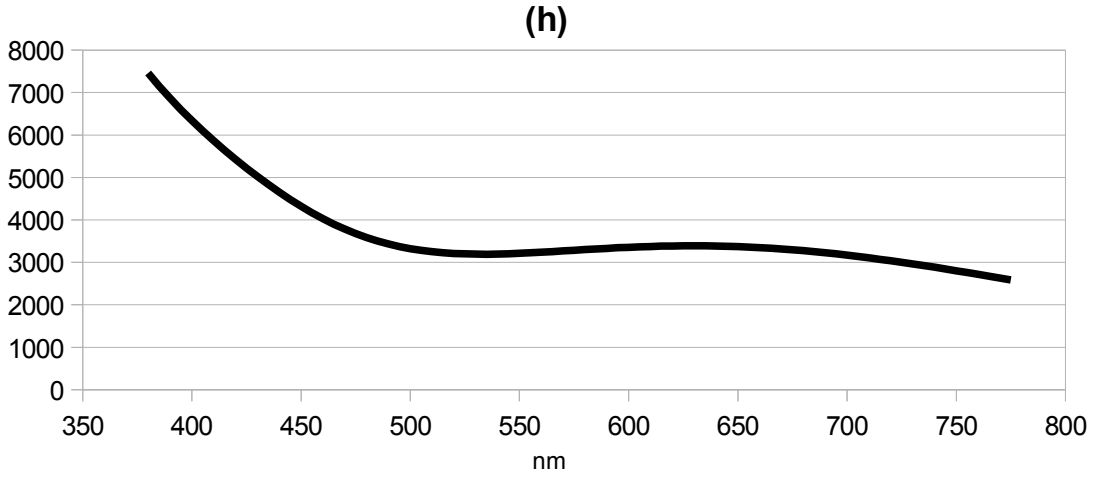

Table 3 – CIE1931 Chromacity Coordinates for the Ruthenium Chloride Clusters

Cluster	CIE1931 Chromacity Coordinates		Physically Interpreted Colour
	x	*y*	
$[Ru_5Cl_{12}]^-$	0.351	0.370	Yellow
$[Ru_4Cl_{11}]^-$	0.223	0.116	Blue
$[Ru_3Cl_9]^-$	0.369	0.381	Yellow
$[Ru_3Cl_8]^-$	0.436	0.445	Orange
$[Ru_2Cl_7]^-$	0.365	0.345	Yellow
$[Ru_2Cl_6]^-$	0.376	0.405	Yellow
$[RuCl_5]^-$	0.491	0.463	Orange
$[RuCl_4]^-$	0.380	0.409	Yellow

Figure 27 – Plot of Chromacity Coordinates of the Clusters on the CIE1931 Gamut

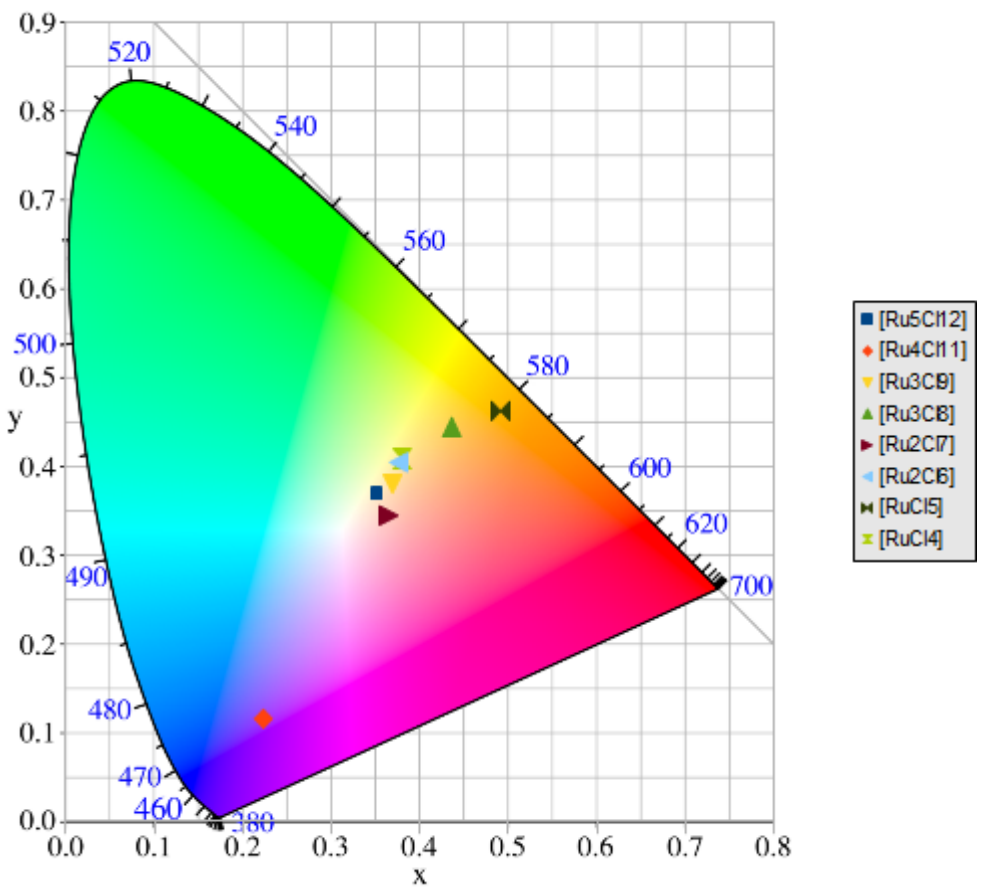

3.4 Calculated Electronic Excitation Spectra of the Blue Compound

The yellow solution of the blue compound has a composition of the clusters $[RuCl_4]^-$ to $[Ru_2Cl_6]^-$. When overlapping their UV/Vis spectra, the resulting perceived colour was a yellow/orange and is representative of the experimental findings. When overlapping the UV/Vis spectra of the whole set of clusters from $[RuCl_4]^-$ to $[Ru_5Cl_{12}]^-$, the physically perceived colour is blue which is again representative of the experimental findings. Since the green solution of the blue compound shows the presence of all the clusters, a UV/Vis spectrum overlap for the green stage is omitted. The respective UV/Vis spectra of the various solutions is seen in *Figure 28*. The CIE1931 chromacity coordinates of the various solutions is seen in *Table 4* and their location in colour space can be seen in *Figure 29*.

Figure 28 – Calculated UV/Vis spectra of the Solutions. (a) Blue and (b) Yellow

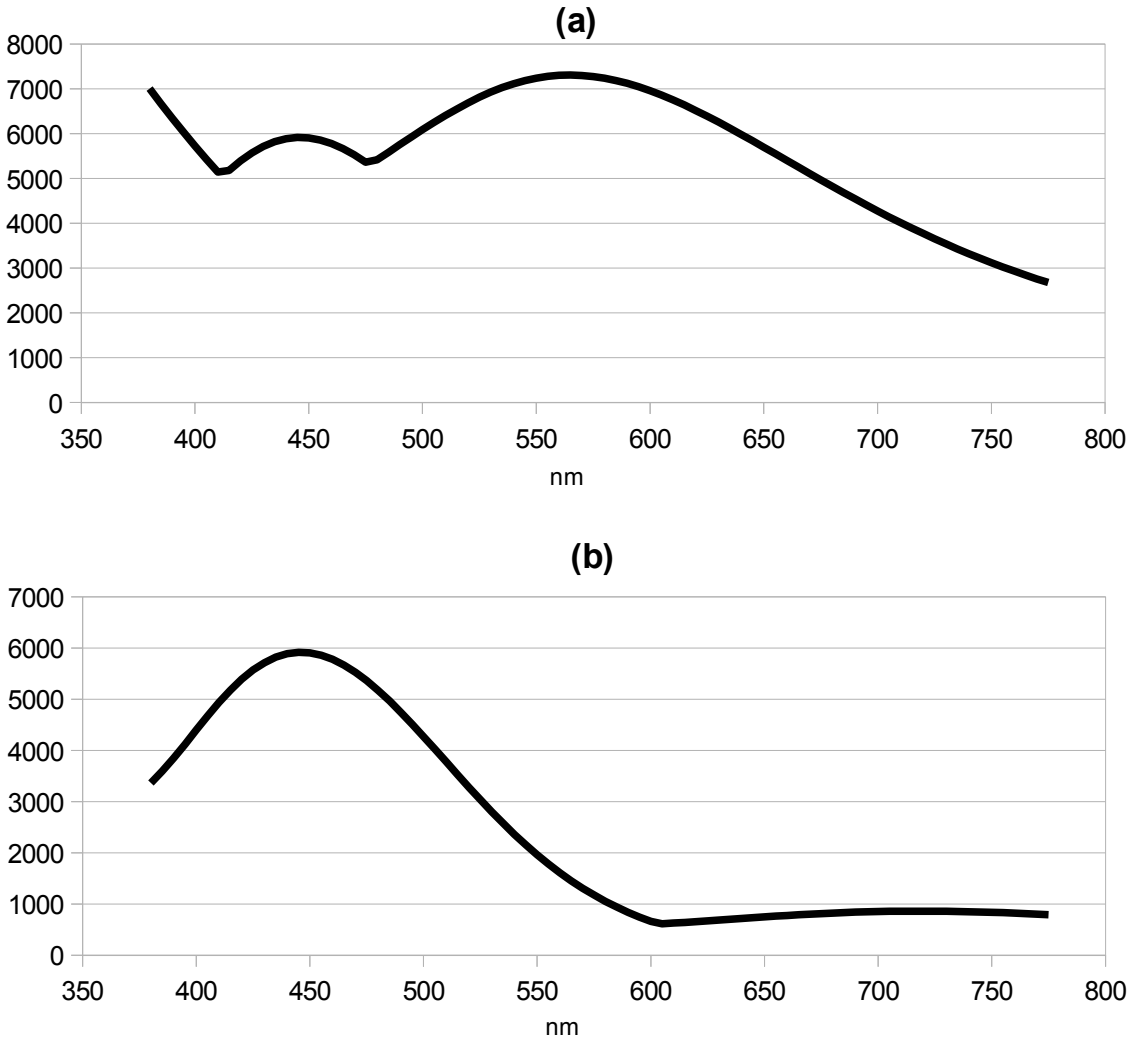

Table 4 – CIE1931 Chromacity Coordinates of the Solutions

Cluster	CIE1931 Chromacity Coordinates		Physically Interpreted Colour
	x	*y*	
Blue	0.255	0.167	Blue
Yellow	0.487	0.467	Yellow/Orange

Figure 29 – Plot of Chromacity Coordinates of the Blue and Yellow Solutions on the CIE1931 Gamut

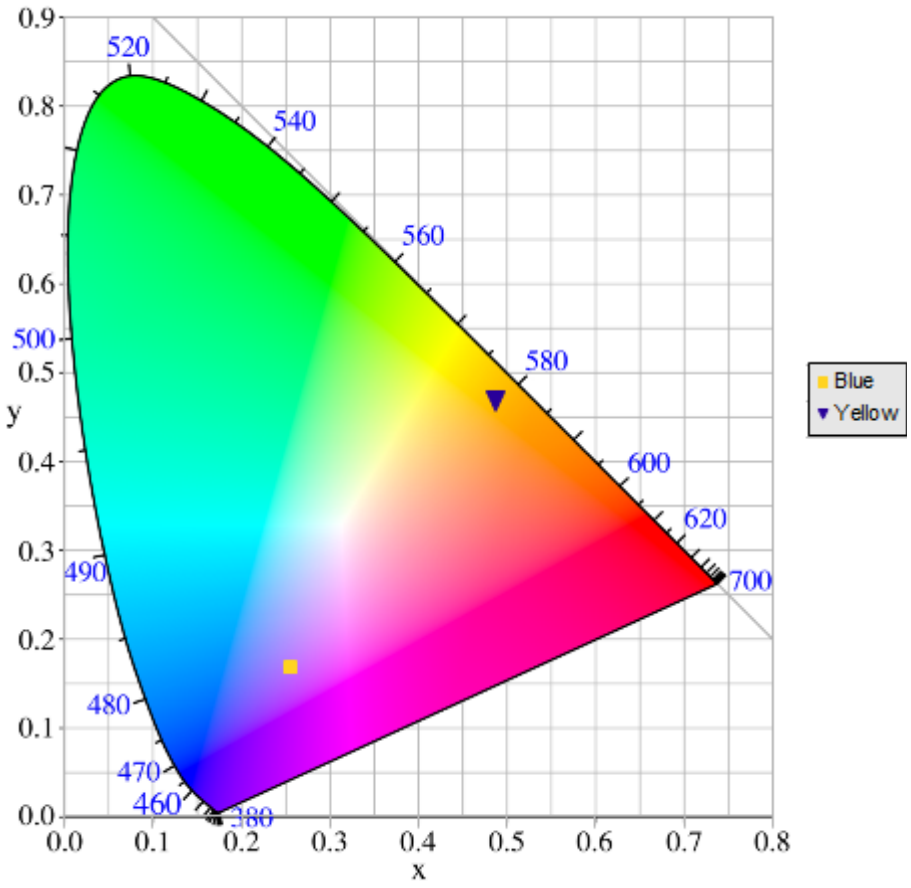

3.5 - Calculated Electronic Excitation Spectra of other Ruthenium Halides

One of the ways to test the validity of this colour interpretation method is to test whether or not the colour of other know and similar in composition compounds can be predicted through the same method. Therefore a sufficient method for testing would be to determine the colour of other ruthenium halide species. Ruthenium fluoride (RuF_4), Ruthenium Chloride ($RuCl_3$) and Ruthenium Bromide ($RuBr_3$) are all known and even commercially available compounds. RuF_4 is described as a deep pink colour[33], while $RuCl_3$ and $RuBr_3$ are both described as deep orange solids. *Figure 30* shows the calculated UV/Vis absorption spectra of the ruthenium halide compounds.

Figure 30 – UV/Vis absorption spectra of a) RuF_4 b) $RuCl_3$ c) $RuBr_3$

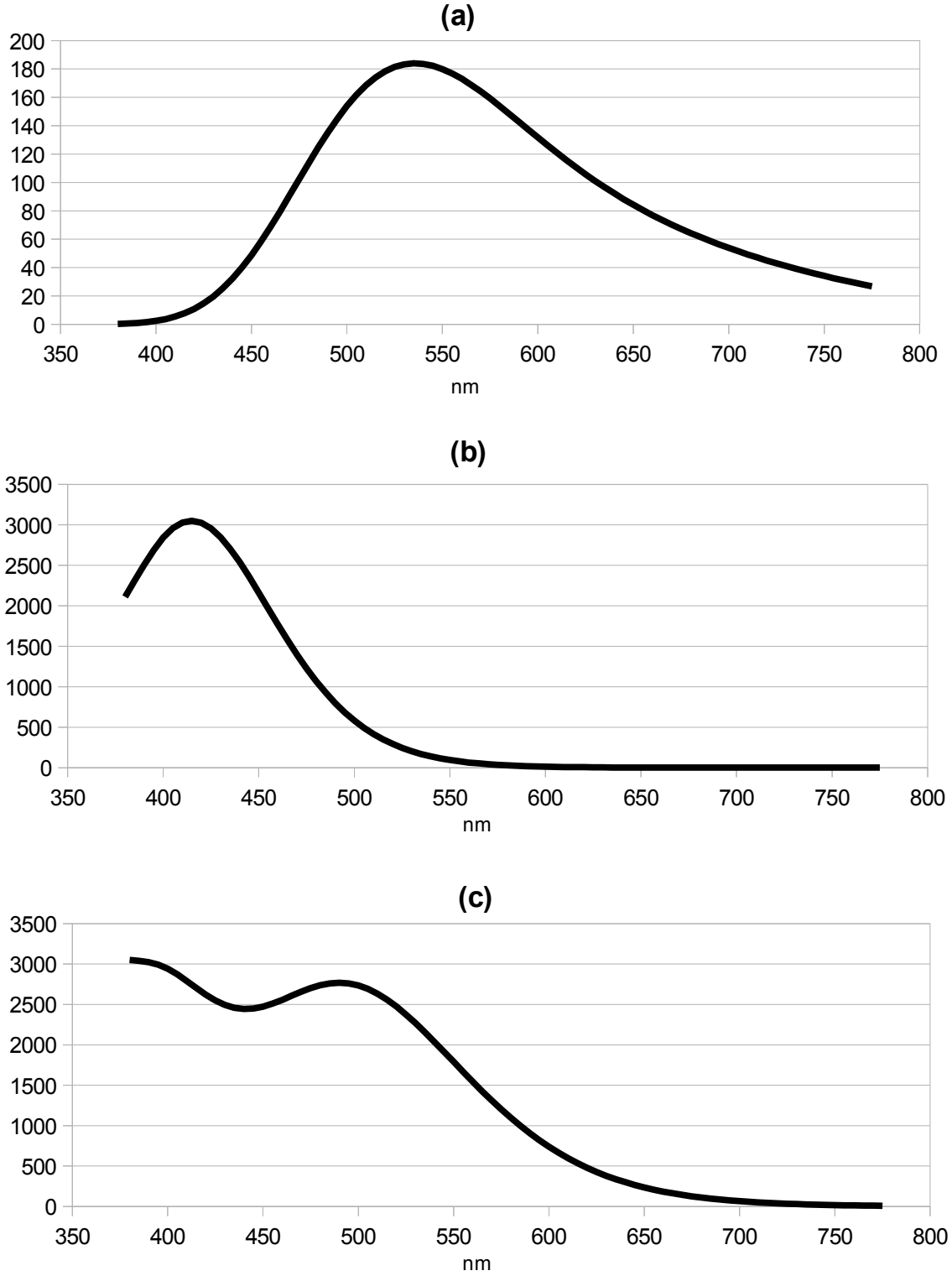

The absorption spectra transformed and plotted on CIE1931 Colour Space is shown in *Figure 31*.

Figure 31 – RuF_4, $RuCl_3$, $RuBr_3$ plotted on CIE1931 Colour Space

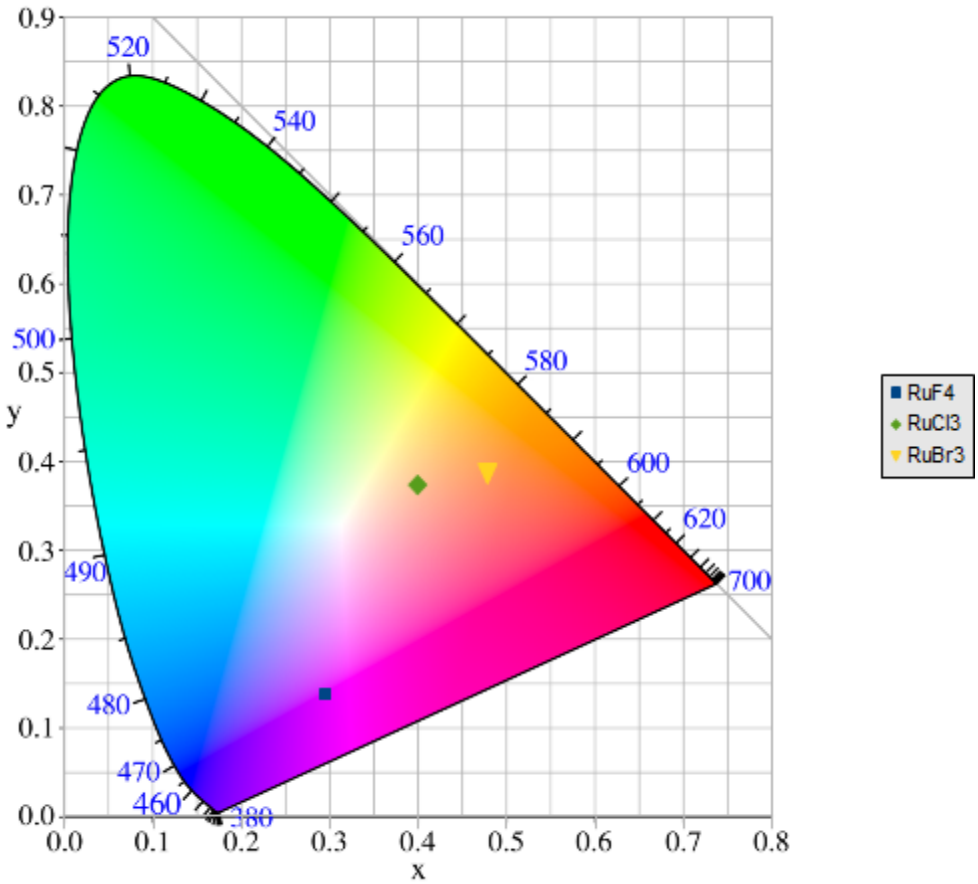

As one can see the physical colour interpretation of RuF_4 is indeed deep pink, $RuCl_3$ is orange and $RuBr_3$ is also orange. These results are in agreement with the physically perceived colour of their respective compounds. Additionally this also shows that the methods used for colour prediction extend beyond that of Ruthenium Chloride species but also into other ruthenium halide species.

Chapter 4: Conclusions and Future Work

The colour sequence of the Ruthenium Blue degrading from the original blue, to green and finally at yellow can be attributed to the decomposition of the $[Ru_4Cl_{11}]^-$ species. With no decomposition occurring, a fresh sample of the blue substance would get the physically perceived blue hue from the compound with the highest extinction coefficient, $[Ru_4Cl_{11}]^-$. The UV/Vis spectrum with the contribution from $[Ru_4Cl_{11}]^-$ highlighted is seen in *Figure 32*.

Figure 32 – UV/Vis spectrum of the Blue Solution with the Contribution from $[Ru_4Cl_{11}]^-$ highlighted

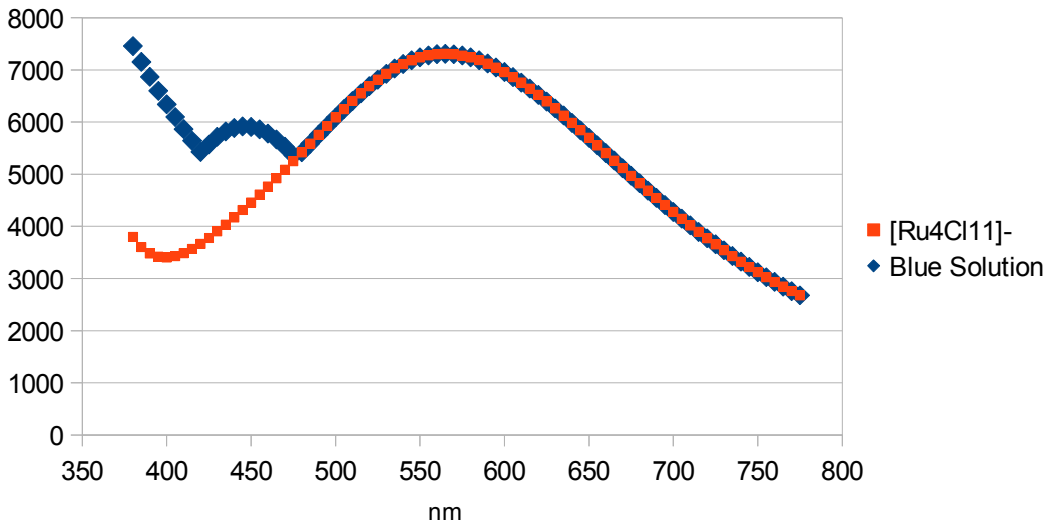

As $[Ru_4Cl_{11}]^-$ begins to degrade, the yellow hues generated from the remaining clusters start to become dominant, shifting the colour from blue to yellow. In colour theory, the addition of blue to yellow produces a green. It is thought that the transitional green coloured solution is produced by “equal amounts” of blue character from $[Ru_4Cl_{11}]^-$ and yellow character from the remaining clusters. Once $[Ru_4Cl_{11}]^-$ has completely degraded the yellow character

of the other clusters become the dominant hues making the resulting solution appear as yellow. The prediction for the colour of the ruthenium chloride clusters, and those of the standards, have been remarkably accurate for the simplicity of the methodology. The findings from this project reinforces the legitimacy computational chemistry as a powerful tool for determining experimental properties to highly unusual chemical species. As stated previously the composition of the ruthenium coordination precursor Ruthenium Blue and the structure and geometry of the species present in a solution of Ruthenium Blue have never been conclusively determined. This is not surprising given the relatively high instability of Ruthenium Blue which makes any analysis cumbersome and difficult. Decomposition occurs so rapidly that it would be essential for analysis to be performed under an inert atmosphere in order to ensure a non-degraded sample. Based upon the visual characteristics of Ruthenium Blue and the synthesized blue compound from $RuCl_3 \cdot 3H_2O$ and D-(+)-Glucosamine and output generated from *ab initio* calculations, it is proposed that the clusters presented in this thesis be another possibility for the composition of Ruthenium Blue. This is the first report of using mass spectroscopy in tandem with *ab initio* calculations in order to determine the chemical composition of Ruthenium Blue.

The study of Ruthenium Blue and the investigations into the ruthenium chloride clusters is abundant with opportunities for further work. Reactions

involving ruthenium chloride with other saccharides to see if the ruthenium chloride clusters can be detected through MALDI-ToF-MS experiments can also be explored. Monosaccharides can also be further divided, testing between reducing sugars like glucose and galactose and non-reducing sugars like fructose to study the proposed stabilization of reducing sugars on the ruthenium chloride clusters. Experiments involving the use of N-acetylglucose as the monosaccharide of choice would also provide useful information specifically related to our work on bacterial PSs as a number of the polysaccharides in our research contain this monosaccharide.

From a mass spectrometry perspective, using a tandem mass spectrometer such as MALDI-ToF-MS/MS would also provide further evidence of the structure of these ruthenium chloride clusters. By being able to further fragment specific ruthenium chloride clusters, greater evidence for their structure could be obtained. It could be possible that the larger ruthenium chloride clusters would fragment specifically into the lower mass clusters of $[RuCl_4]^-$ and $[RuCl_5]^-$.

Lastly for experimental work, obtaining an x-ray crystallographic structure of the blue compound would definitively prove the structure and species of present in solution. Attempts were made at crystallization of the blue compound but have so far been unsuccessful. Various techniques have been employed in order to obtain crystals of the described blue compound. Non-polar solvents such as

methylene chloride and petroleum ether have been used as a counter-solvent to ethanol solutions of the blue compound. Recrystallization of both diffusion and addition of a counter-solvent have both been unsuccessful in providing crystals of any quality. As well ethanol solutions of the blue compound with magnesium and calcium chloride added for positive counter ions have also been unsuccessful. It is thought that at least some, if not all the clusters, would be able to produce crystals suitable for xray crystallographic analysis.

Future work can also be carried out on the *ab initio* calculations of the ruthenium chloride clusters. With the rapid advancement of computing performance, more accurate and detailed information of the ruthenium chloride clusters can be obtained. Upgrading to an all triple-zeta basis set would be the first improvement to more accurate results. Switching from an SDD basis set on the ruthenium atoms to def2-tzvp basis set would be the way to do this. As well with the success seen in predicting the colour of the other ruthenium halide species, further discoveries could be made in seeing if a series of ruthenium halide clusters can be made from the laser desorption of RuF_4 and $RuBr_3$. While no supporting evidence of literature of the refluxing these ruthenium halide compounds would yield large ruthenium halide clusters, let alone colour determination of the solutions, it could definitely be another fruitful project to investigate.

Chapter 5: References

[1] Credit: Michael Jones. Picture licensed under Creative Commons Attribution-Share Alike 3.0 Unported License.

[2] Heinrichs, D. E.; Yethon, J. A.; Whitfield, C. *Molecular Microbiology* 1998, **30** (2): 221–232.

[3] Raetz, C.; Whitfield, C. *Annu. Rev. Biochem.* 2001, **71**: 635-700.

[4] Tortora, G.J.; Funke, B.R.; Case, C.L. Microbiology: An Introduction. 8th ed. London: Benjamin Cummings, 2003.

[5] Blakeney, A.B.; Harris, P.J.; Henry, R.J.; Stone, B.A. *Carbohydr. Res.* 1983, **113** (2): 291-299.

[6] Anumula, K.R.; Taylor, P.B. *Anal. Biochem.* 1992, **203** (1): 101-108.

[7] Bruker AG. ADVANCE Users Manual. Fällanden, Switzerland, 2000.

[8] Woods, Robert J. "The Application of Molecular Modeling Techniques to the Determination of Oligosaccharide Solution Conformations." in Reviews of Computational Chemistry, Volume 9., 129-165. ed. Kenny B. Lipkowitz and Donald B. Boyd. New Jersey: John Wiley &Sons, Inc., 1996.

[9] Allscher, T.; Klüfers, P.; Mayer, P. *Glycoscience* 2008, (4): 1077-1139.

[10] Steinborn, D; Junicke, H. *Chem. Rev.* 2000, (100): 4283-4317.

[11] Geetha, K.; Raghavan, M. S. S.; Kulshreshtha, S. K.; Sasikala, R.; Rao, C. P. *Carbohydr. Res.* 1995, **271** (2): 163-175.

[12] Schwarz, T.; Heß, D.; Klufers, P. *Dalton Trans.* 2010, **39** (23): 5544-5555.

[13] Striegler, S.; Dittel, M. *Inorg. Chem.* 2005, **44** (8): 2728-2733.

[14] Gilbert, J.D.; Rose, D.; Wilkinson, G. *J. Chem. Soc. (A).* 1970, 2765-2769.

[15] Rose, D.; Wilkinson, G. *J. Chem. Soc. (A).* 1970**,** 1791-1795.

[16] Mercer, E.E.; Dumas, P.E. *Inorg. Chem.* 1971, **10** (12): 2755-2759.

[17] Togano, T.; Nagao, N.; Tsuchida, M.; Kumakura, H.; Hisamatsu, K.; Howell, F.S.; Mukaida, M. *Inorg. Chim. Acta.* 1992, **195**: 221-225.

[18] Bino, A.; Cotton, F.A. *J. Am. Chem. Soc.* 1980, **102** (2): 608-611.

[19] Schanda, J., ed. Colorimetry: Understanding the CIE System. Hoboken: John Wiley and Sons, Inc., 2007.

[20] Guild, J. *Phil. Trans. Royal. Soc. London. (A).* 1932, **230**: 149-187.

[21] Wyszecki, G.; Stiles, W.S. Color Science: Concepts and Methods, Quantitative Data and Formulae. 2nd ed. New York: John Wiley and Sons, Inc., 1982.

[22] Mortimer, R.J.; Varley, T.S. *Displays*. 2011, **32**: 35-44.

[23] Beck, M.E. *Int. J. Quan. Chem.* 2005, **101**: 683-689.

[24] Hehre, W.J.; Stewart, R.F.; Pople, J.A. *J. Chem. Phys.* 1969, **51** (6): 2657-2664.

[25] Andrae, D.; Häussermann, U.; Dolg, M.; Stoll, H.; Preuss, H. *Theor. Chim. Acta.* 1990, **77** (2): 123-141.

[26] McLean, A.D.; Chandler, G.S. *J. Chem. Phys.* 1980, **72** (10): 5639-5649.

[27] Tomasi, J.; Mennucci, B.; Cances, E. *J. Mol. Struct. (Theochem)* 1999, **464** (1-3): 211-226.

[28] Gorelsky, S. I. *AOMix: Program for Molecular Orbital Analysis,* version 6.4; University of Ottawa; Ottawa, ON, 2010. http://www.sg-chem.net.

[29] Gorelsky, S.I.; Lever, A.B.P. *J. Organomet. Chem.* **635** (1-2): 187-196.

[30] Frisch, M. J.; Trucks, G. W.; Schlegel, H. B.; Scuseria, G.E.; Robb, M. A.; Cheeseman, J. R.; Scalmani, G.; Barone, V.; Mennucci, B.; Petersson, G. A.; Nakatsuji, H.; Caricato, M.; Li, X.; Hratchian, H. P.; Izmaylov, A. F.; Bloino, J.; Zheng, G.; Sonnenberg, J. L.; Hada, M.; Ehara, M.; Toyota, K.; Fukuda, R.; Hasegawa, J.; Ishida, M.; Nakajima, T.; Honda, Y.; Kitao, O.; Nakai, H.; Vreven, T.; Montgomery,

J. A., Jr.; Peralta, J. E.; Ogliaro, F.; Bearpark, M.; Heyd, J. J.; Brothers, E.; Kudin, K. N.; Staroverov, V. N.; Kobayashi, R.; Normand, J.; Raghavachari, K.; Rendell, A.; Burant, J. C.; Iyengar, S. S.; Tomasi, J.; Cossi, M.; Rega, N.; Millam, J. M.; Klene, M.; Knox, J. E.; Cross, J. B.; Bakken, V.; Adamo, C.; Jaramillo, J.; Gomperts, R.; Stratmann, R. E.; Yazyev, O.; Austin, A. J.; Cammi, R.; Pomelli, C.; Ochterski, J. W.; Martin, R. L.; Morokuma, K.; Zakrzewski, V. G.; Voth, G. A.; Salvador, P.; Dannenberg, J. J.; Dapprich, S.; Daniels, A. D.; Farkas, O.; Foresman, J. B.; Ortiz, J. V.; Cioslowski, J.; Fox, D. J. *Gaussian 09,* Revision A.02; Gaussian, Inc.: Wallingford, CT, 2009.

[31] Oracle. *OpenOffice,* version 3.2; http://www.openoffice.org.

[32] Boncheff, A.G.; Monteiro, M.A. *Can. J. Chem.* 2011, **89** (4): 511-516.

[33] Cotton, S.A. Chemistry of Precious Metals. London: Chapman & Hall, 1997. pp 3-5.

Chapter 6: Appendix

6.1 Input Files for the TDDFT Calculations of the Ruthenium Chloride Clusters

Input File for TDDFT Calculation for the UV/Vis Spectrum of $[RuCl_4]^-$

```
%rwf=RuCl4-tddft-solv.rwf
%nosave
%chk=RuCl4-tddft-solv.chk
%nprocshared=16
#p td=(nstates=30)/genecp scrf=(solvent=water) geom=connectivity pbe1pbe

Title Card Required

-1 4
 Ru                 0.00000100   -0.00001200   -0.00002100
 Cl                -2.13355500   -0.89362600   -0.06221700
 Cl                 0.89364500   -2.13347000    0.06225500
 Cl                 2.13354500    0.89372200   -0.06206800
 Cl                -0.89365000    2.13355600    0.06209300

 1 2 1.0 3 1.0 4 1.0 5 1.0
 2
 3
 4
 5

Cl     0
6-311g(2d,p)
****
Ru     0
SDD
****

Ru     0
SDD
```

Input File for TDDFT Calculation for the UV/Vis Spectrum of $[RuCl_5]^-$

```
%rwf=RuCl5-tddft-solv.rwf
%nosave
%chk=RuCl5-tddft-solv.chk
%nprocshared=16
#p td=(nstates=55)/genecp scrf=(solvent=water) geom=connectivity pbe1pbe

Title Card Required

-1 5
 Ru                 0.00006500    0.00002900   -0.15582900
 Cl                 2.21637400    0.57461300   -0.46277000
 Cl                -0.57456800    2.21586500   -0.46625200
 Cl                 0.57475200   -2.21583700   -0.46601300
 Cl                -0.00110900   -0.00008300    2.26240600
 Cl                -2.21561700   -0.57463200   -0.46404900

 1 2 1.0 3 1.0 4 1.0 6 1.0
 2
 3
 4
 5
 6

Cl     0
6-311g(2d,p)
****
Ru     0
SDD
****

Ru     0
SDD
```

Input File for TDDFT Calculation for the UV/Vis Spectrum of $[Ru_2Cl_6]^-$

```
%rwf=Ru2Cl6-tddft-solv.rwf
%nosave
%chk=Ru2Cl6-tddft-solv.chk
%nprocshared=16
#p td=(nstates=80)/genecp scrf=(solvent=water) geom=connectivity pbe1pbe

Title Card Required

-1 4
 Ru                 1.16207100    0.13148100    0.25131500
 Ru                -1.16834300   -0.16246400    0.25854400
 Cl                 0.23979800   -1.70320400    1.52444400
 Cl                -1.97197200   -1.85679400   -1.06695900
 Cl                 2.27218100   -1.29527600   -1.15953600
 Cl                 1.88765100    1.98410300   -0.88465400
 Cl                -0.17131000    1.51717600    1.72025000
 Cl                -2.20590000    1.42920400   -1.04075600

 1 2 1.0 5 1.0 6 1.0
 2 4 1.0 8 1.0
 3
 4
 5
 6
 7
 8

Cl     0
6-311g(2d,p)
****
Ru     0
SDD
****

Ru     0
SDD
```

Input File for TDDFT Calculation for the UV/Vis Spectrum of $[Ru_2Cl_7]^-$

```
%rwf=Ru2Cl7-tddft-solv.rwf
%nosave
%chk=Ru2Cl7-tddft-solv.chk
%nprocshared=16
#p td=(nstates=95)/genecp scrf=(solvent=water) pbe1pbe

Title Card Required

-1 5
 Ru,0,0.0675754883,-0.0697842013,-0.6524804452
 Ru,0,0.2577529034,-0.0030067407,2.2758266423
 Cl,0,1.7132923093,-0.0407961808,-2.2570211459
 Cl,0,-1.2670346298,-1.3925413361,-1.9763805253
 Cl,0,-1.6330644716,-0.0496504044,1.0400847333
 Cl,0,1.1854550599,1.5884562213,0.6528815793
 Cl,0,1.1081343705,-1.7885124111,0.9690205152
 Cl,0,-0.5355192774,-1.5046954292,3.8529164983
 Cl,0,-0.3222489618,1.7748455861,3.6290752021

Cl     0
6-311g(2d,p)
****
Ru     0
SDD
****

Ru     0
SDD
```

Input File for TDDFT Calculation for the UV/Vis Spectrum of $[Ru_3Cl_8]^-$

```
%mem=20GB
%rwf=Ru3Cl8-tddft-solv.rwf
%nosave
%chk=Ru3Cl8-tddft-solv.chk
%nprocshared=16
#p td=(nstates=135)/genecp scrf=(solvent=water) geom=connectivity pbe1pbe

Title Card Required

-1 2
 Ru                -1.45082200    0.00130000   -0.10166300
 Ru                 0.75022000    1.22093100    0.17403400
 Ru                 0.77892300   -1.22437000    0.16458600
 Cl                 2.01556100    0.04813700    1.81357300
 Cl                -1.05313300   -1.61647600    1.59892100
 Cl                -0.74024500   -1.71748000   -1.58485400
 Cl                 2.66139100   -1.79227400   -0.95406000
 Cl                -1.09369300    1.68415900    1.57150400
 Cl                 2.53528600    1.79563800   -1.06460800
 Cl                -0.79034800    1.72557600   -1.59169200
 Cl                -3.73753100   -0.12174200   -0.40208500

 1 2 1.0 3 1.0 11 1.0
 2 3 1.0 8 1.0 9 1.0
 3 5 1.0 7 1.0
 4
 5
 6
 7
 8
 9
 10
 11

Cl     0
6-311g(2d,p)
****
Ru     0
SDD
****

Ru     0
SDD
```

Input File for TDDFT Calculation for the UV/Vis Spectrum of $[Ru_3Cl_9]^-$

```
%mem=20GB
%rwf=Ru3Cl9-tddft-solv.rwf
%nosave
%chk=Ru3Cl9-tddft-solv.chk
%nprocshared=16
#p td=(nstates=170)/genecp scrf=(solvent=water) geom=connectivity pbe1pbe

Title Card Required

-1 3
 Ru                 0.00000200    1.50482600   -0.46287700
 Ru                 1.28762100   -0.55745800    0.03364600
 Ru                -1.28762100   -0.55745700    0.03364200
 Cl                -2.34148800    1.47836800   -0.53164300
 Cl                 0.00000200   -0.31933000   -2.15813000
 Cl                 0.00000100    3.29412900    0.90236800
 Cl                 2.34149200    1.47836400   -0.53163500
 Cl                -3.02321800   -1.84198100   -0.75758600
 Cl                -1.95273500   -0.39888500    2.17591700
 Cl                -0.00000200   -2.45897000    0.50626100
 Cl                 3.02321000   -1.84198700   -0.75759500
 Cl                 1.95273000   -0.39889000    2.17592200

 1 2 1.0 3 1.0 4 1.0 6 1.0 7 1.0
 2 3 1.0 7 1.0 10 1.0 11 1.0 12 1.0
 3 4 1.0 8 1.0 9 1.0 10 1.0
 4
 5
 6
 7
 8
 9
 10
 11
 12

Cl     0
6-311g(2d,p)
****
Ru     0
SDD
****

Ru     0
SDD
```

Input File for TDDFT Calculation for the UV/Vis Spectrum of $[Ru_4Cl_{11}]^-$

```
%rwf=Ru4Cl11-tddft-solv.rwf
%nosave
%chk=Ru4Cl11-tddft-solv.chk
%nprocshared=16
%mem=20GB
#p td=(nstate=210) pbe1pbe/genecp scrf=(solvent=water)

Molecule Name

-1 7
 Ru,0,-2.7452218915,-0.096706825,-0.2091484841
 Ru,0,0.0726916404,1.7373091479,-0.1848548599
 Ru,0,-0.5286686645,-1.1912778466,-0.3286173874
 Ru,0,2.2515955257,-0.4915614441,0.0662670015
 Cl,0,-2.2660409231,-2.1968165925,0.9116826266
 Cl,0,-0.4097708962,3.4662638205,1.237445034
 Cl,0,1.4262489838,-2.6994236992,-0.3963324348
 Cl,0,3.6997792446,-1.0934049271,1.7580844561
 Cl,0,0.4899323879,-0.503864559,1.7348690785
 Cl,0,2.3851216307,1.8668636825,0.439706065
 Cl,0,-2.1449019254,1.9655246382,-1.2356506586
 Cl,0,-2.0672913001,-1.4215251426,-2.144343185
 Cl,0,0.8012923411,0.1397823193,-1.846460889
 Cl,0,3.9910021422,-0.5524927918,-1.4703823182
 Cl,0,-3.5020612955,0.9280592198,1.6976049555

Cl     0
6-311g(2d,p)
****
Ru     0
SDD
****

Ru     0
SDD
```

Input File for TDDFT Calculation for the UV/Vis Spectrum of $[Ru_5Cl_{12}]^-$

```
%mem=21GB
%rwf=Ru5Cl12-tddft-solv.rwf
%nosave
%chk=Ru5Cl12-tddft-solv.chk
%nprocshared=16
#p td(nstates=300) genecp scrf=(solvent=water) pbe1pbe

Title Card Required

-1 8
 Ru,0,2.0340041628,1.1945581384,-0.2982879777
 Ru,0,1.2861244968,-1.1037973528,-0.3911287573
 Ru,0,-2.1389505054,-1.1836714115,-0.3131044802
 Ru,0,-1.1254862008,1.0312787029,-0.4288971394
 Cl,0,0.4045906725,2.8674103451,-0.9160037344
 Cl,0,1.7979985953,0.1015174079,-2.4363414221
 Cl,0,-0.4093563237,-2.7896749635,-0.806316635
 Cl,0,-1.6687415489,-0.1998031143,-2.4589964209
 Cl,0,4.267671875,0.6876521816,-0.0738795901
 Cl,0,2.9824172336,-2.5591825408,-0.8863360194
 Cl,0,-4.3704227795,-0.6355500815,-0.1460703427
 Cl,0,-2.8751455251,2.418034483,-1.0310346768
 Ru,0,-0.0382546536,0.0327361024,1.8192765252
 Cl,0,1.8601028042,1.4865842293,2.0664545178
 Cl,0,1.3677116951,-1.8534953523,1.85809389
 Cl,0,-1.428635431,1.9171624179,1.7650656994
 Cl,0,-1.9704475672,-1.3827371916,2.0671165637

Cl     0
6-311g(2d,p)
****
Ru     0
SDD
****

Ru     0
SDD
```

6.2 Cartesian Coordinates of Geometry Optimized Ruthenium Chloride Clusters

$RuCl_4$ Coordinates

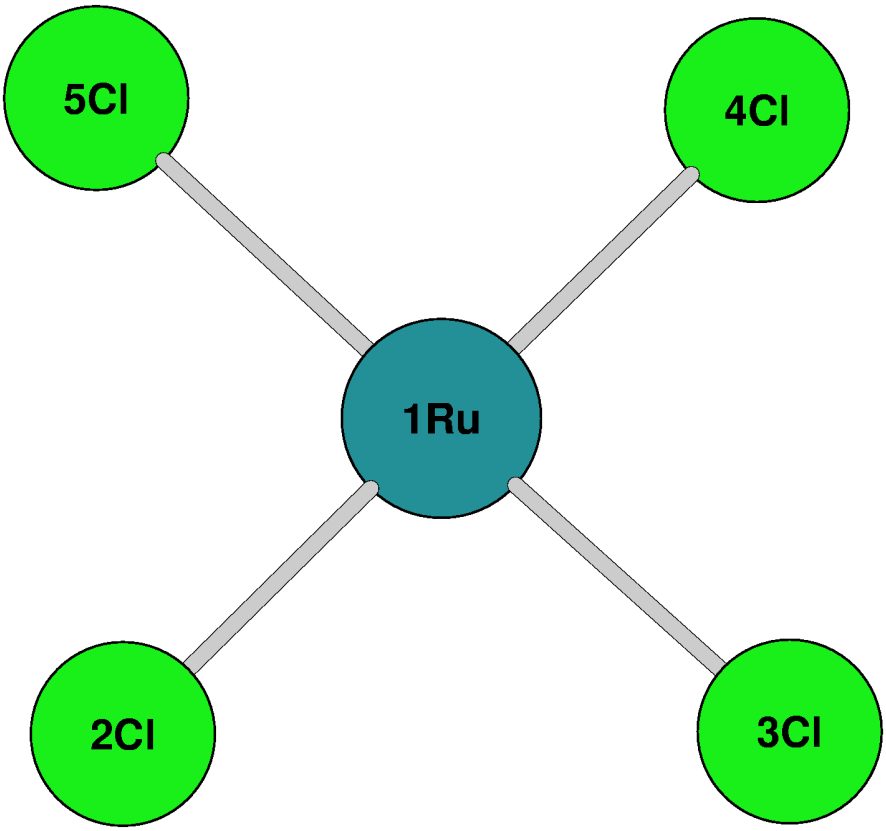

Cartesian Coordinates

Atom	*X*	*Y*	*Z*
1Ru	0.000014	0.000032	-0.000022
2Cl	2.298548	-0.259491	-0.062218
3Cl	0.259464	2.298494	0.062254
4Cl	-2.298567	0.259444	-0.062069
5Cl	-0.259482	-2.298530	0.062092

$RuCl_5$ Coordinates

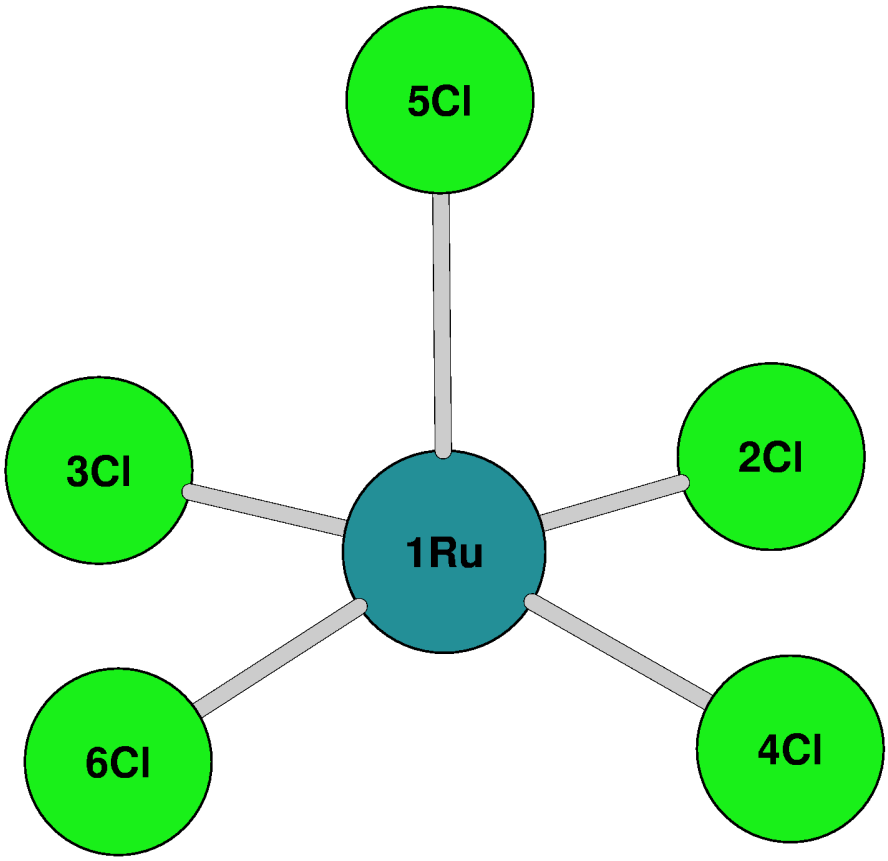

Cartesian Coordinates

Atom	*X*	*Y*	*Z*
1Ru	0.000100	0.000000	-0.155800
2Cl	2.216400	0.574700	-0.462800
3Cl	-0.574600	2.215900	-0.466300
4Cl	0.574800	-2.215800	-0.466000
5Cl	-0.001100	-0.000100	2.262400
6Cl	-2.215600	-0.574700	-0.464000

Ru_2Cl_6 Coordinates

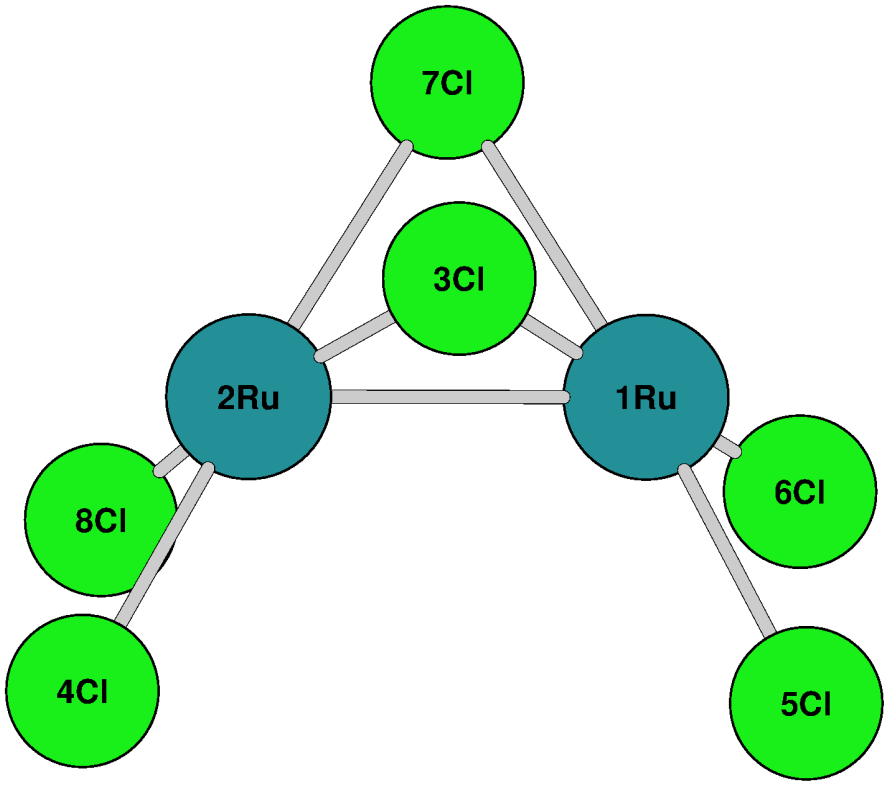

Cartesian Coordinates

Atom	*X*	*Y*	*Z*
1Ru	1.166400	-0.070300	0.202900
2Ru	-1.178800	0.057200	0.234000
3Cl	-0.053000	-1.668200	1.543500
4Cl	-2.287400	-1.508700	-1.028000
5Cl	1.987400	-1.717700	-1.164800
6Cl	2.197200	1.584800	-1.000000
7Cl	0.119100	1.578500	1.631400
8Cl	-1.931300	1.765300	-1.112900

Ru_2Cl_7 Coordinates

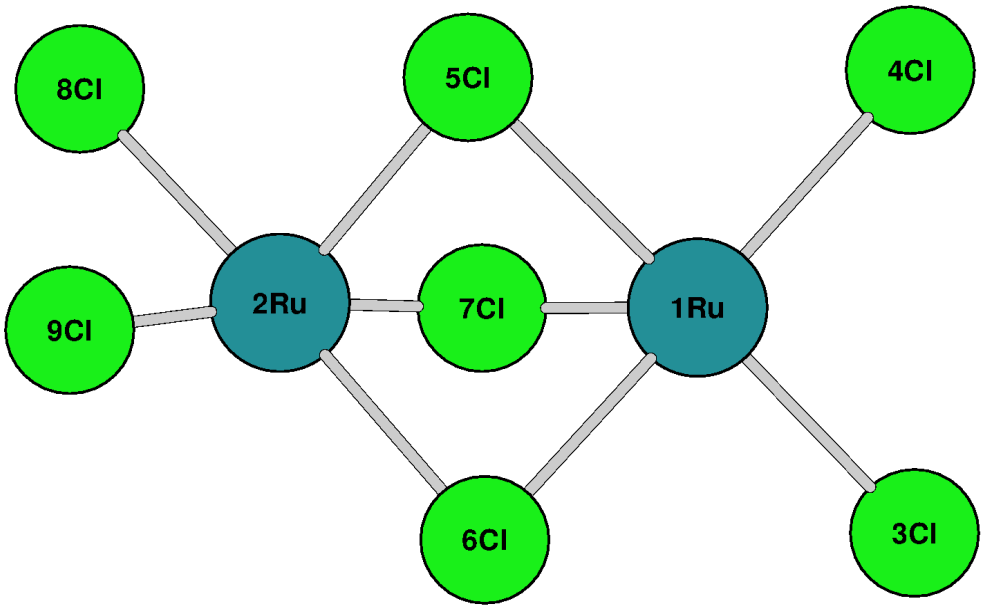

Cartesian Coordinates

Atom	*X*	*Y*	*Z*
1Ru	1.455700	0.108500	-0.269200
2Ru	-1.426000	0.131700	0.288300
3Cl	3.204400	1.076500	0.866000
4Cl	2.782600	-1.657700	-0.904400
5Cl	-0.391200	-0.851000	-1.463200
6Cl	0.086100	2.045300	0.006800
7Cl	0.159400	-0.872200	1.736700
8Cl	-2.889500	-1.632600	0.629900
9Cl	-3.028900	1.270000	-0.921300

Ru_3Cl_8 Coordinates

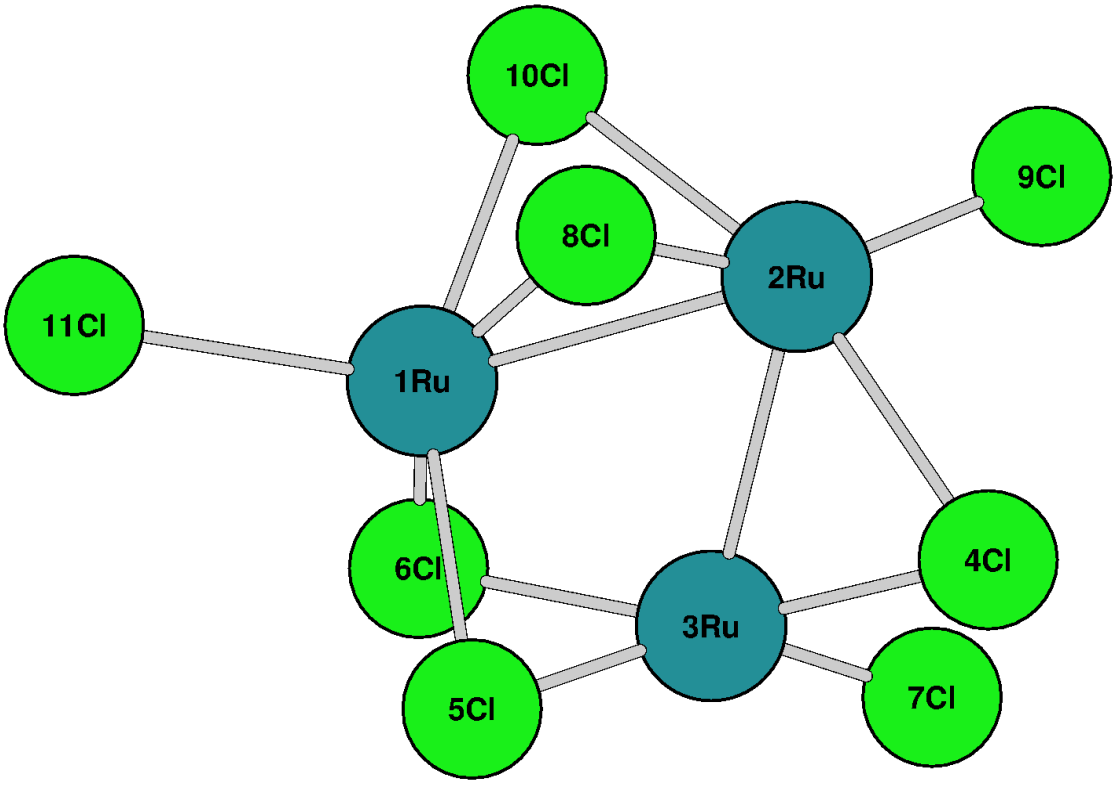

Cartesian Coordinates

Atom	*X*	*Y*	*Z*
1Ru	-1.450800	0.001300	-0.101700
2Ru	0.750200	1.220900	0.174000
3Ru	0.778900	-1.224400	0.164600
4Cl	2.015600	0.048100	1.813600
5Cl	-1.053100	-1.616500	1.598900
6Cl	-0.740200	-1.717500	-1.584900
7Cl	2.661400	-1.792300	-0.954100
8Cl	-1.093700	1.684200	1.571500
9Cl	2.535300	1.795600	-1.064600
10Cl	-0.790300	1.725600	-1.591700
11Cl	-3.737500	-0.121700	-0.402100

Ru_3Cl_9 Coordinates

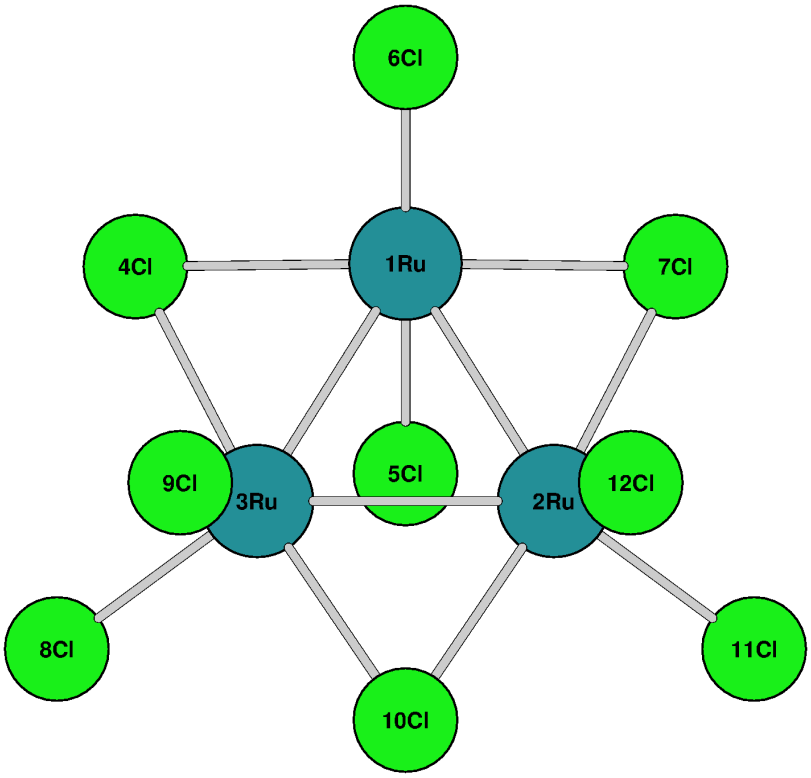

Cartesian Coordinates

Atom	*X*	*Y*	*Z*
1Ru	0.000000	1.504800	-0.462900
2Ru	1.287600	-0.557500	0.033600
3Ru	-1.287600	-0.557500	0.033600
4Cl	-2.341500	1.478400	-0.531600
5Cl	0.000000	-0.319300	-2.158100
6Cl	0.000000	3.294100	0.902400
7Cl	2.341500	1.478400	-0.531600
8Cl	-3.023200	-1.842000	-0.757600
9Cl	-1.952700	-0.398900	2.175900
10Cl	-0.000000	-2.459000	0.506300
11Cl	3.023200	-1.842000	-0.757600
12Cl	1.952700	-0.398900	2.175900

Ru_4Cl_{11} Coordinates

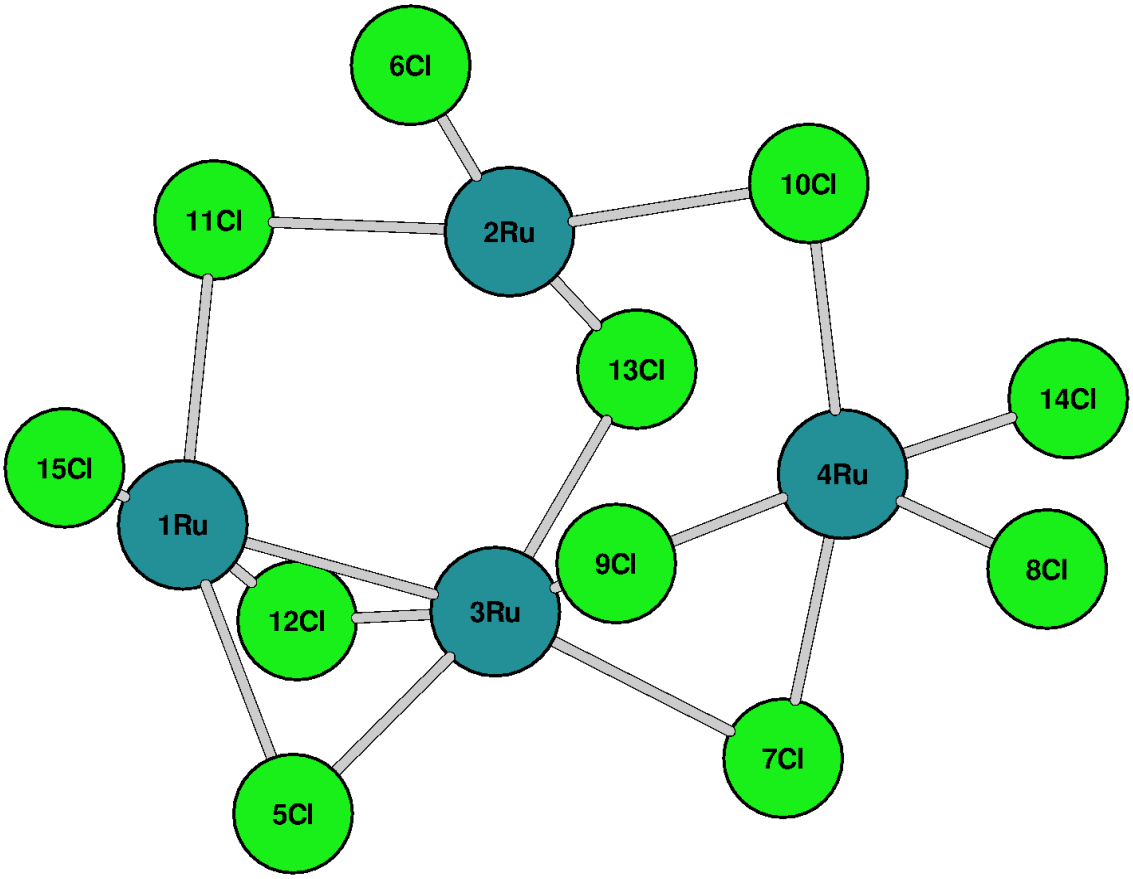

Cartesian Coordinates

Atom	*X*	*Y*	*Z*
1Ru	-2.707100	-0.474000	-0.050800
2Ru	-0.163300	1.688900	-0.445000
3Ru	-0.364100	-1.271400	-0.051100
4Ru	2.299600	-0.153200	0.120100
5Cl	-1.937000	-2.258400	1.404900
6Cl	-0.861100	3.565700	0.666700
7Cl	1.776100	-2.497100	0.081200
8Cl	3.832700	-0.247200	1.841200
9Cl	0.572600	-0.098300	1.823600
10Cl	2.116400	2.230800	0.068300

11Cl	-2.401700	1.432100	-1.443700
12Cl	-1.875500	-2.022700	-1.744800
13Cl	0.758200	-0.070100	-1.823500
14Cl	4.015900	-0.258700	-1.440000
15Cl	-3.576700	0.766700	1.670600

Ru_5Cl_{12} Coordinates

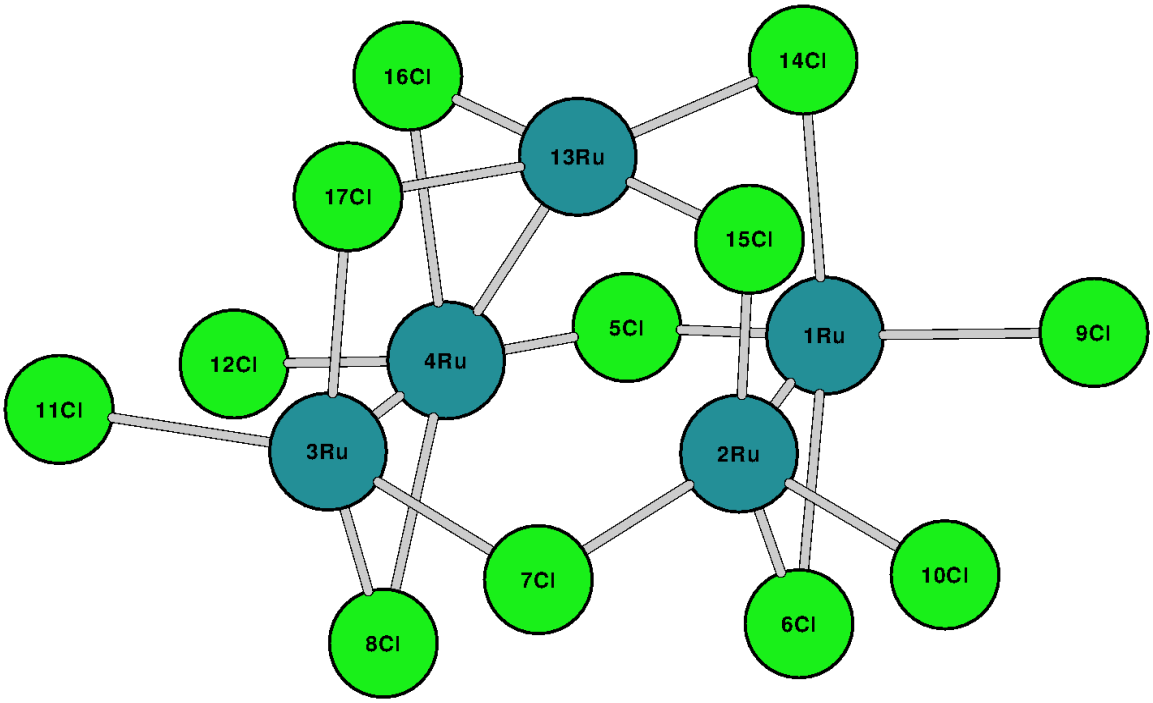

Cartesian Coordinates

Atom	*X*	*Y*	*Z*
1Ru	2.041800	1.181700	-0.298500
2Ru	1.278700	-1.111600	-0.391400
3Ru	-2.146900	-1.168800	-0.313300
4Ru	-1.118700	1.039400	-0.429100
5Cl	0.423500	2.865300	-0.916200
6Cl	1.798500	0.090300	-2.436600
7Cl	-0.428000	-2.786200	-0.806500
8Cl	-1.670100	-0.188000	-2.459200
9Cl	4.272000	0.660000	-0.074100
10Cl	2.965200	-2.578300	-0.886600
11Cl	-4.374700	-0.605800	-0.146300
12Cl	-2.859100	2.437700	-1.031300

13Ru	-0.038100	0.033700	1.819100
14Cl	1.869800	1.474900	2.066200
15Cl	1.355300	-1.861900	1.857900
16Cl	-1.416000	1.927300	1.764800
17Cl	-1.979700	-1.368900	2.066900

6.3 Raw UV/Vis Spectra Data for the Ruthenium Chloride Clusters

UV/Vis Spectrum for $[RuCl_4]^-$

```
# UV-VIS Spectrum
# X-Axis:  Excitation Energy (nm)
# Y-Axis:  Epsilon
#                  X                    Y                DY/DX
      380.0000000000     2382.0840114075       52.4655955851
      385.0000000000     2442.9695549657       60.8005809396
      390.0000000000     2509.2500225839       59.1708375878
      395.0000000000     2564.8199325086       48.6450402703
      400.0000000000     2596.6821889848       31.5257430498
      405.0000000000     2595.9813518708       10.8907659044
      410.0000000000     2558.2704546307      -10.0344437161
      415.0000000000     2483.1750060207      -28.4837449219
      420.0000000000     2373.6568714752      -42.5693539343
      425.0000000000     2235.0773602643      -51.4345831669
      430.0000000000     2074.2274460190      -55.1598607210
      435.0000000000     1898.4476184725      -54.5070678223
      440.0000000000     1714.9118518888      -50.6063078547
      445.0000000000     1530.1074955668      -44.6710969299
      450.0000000000     1349.5098786607      -37.7918978994
      455.0000000000     1177.4284086158      -30.8217465536
      460.0000000000     1016.9891407529      -24.3419999069
      465.0000000000      870.2152056126      -18.6837938644
      470.0000000000      738.1686563154      -13.9792691356
      475.0000000000      621.1228953481      -10.2216035760
      480.0000000000      518.7419258461       -7.3202249219
      485.0000000000      430.2498477565       -5.1444575704
      490.0000000000      354.5804087318       -3.5539353277
      495.0000000000      290.5015848632       -2.4171402065
      500.0000000000      236.7139904185       -1.6207619824
      505.0000000000      191.9244886043       -1.0727759158
      510.0000000000      154.8978982450       -0.7017308654
      515.0000000000      124.4904057619       -0.4541104317
      520.0000000000       99.6684336844       -0.2910062317
      525.0000000000       79.5164901900       -0.1848334971
      530.0000000000       63.2370905001       -0.1164541113
      535.0000000000       50.1453187790       -0.0728377128
      540.0000000000       39.6600684912       -0.0452577099
      545.0000000000       31.2935088492       -0.0279543358
      550.0000000000       24.6399005806       -0.0171747960
      555.0000000000       19.3645350476       -0.0105018763
      560.0000000000       15.1932956212       -0.0063944810
      565.0000000000       11.9031320039       -0.0038790146
      570.0000000000        9.3135869407       -0.0023453921
      575.0000000000        7.2794097566       -0.0014140811
      580.0000000000        5.6842222326       -0.0008504965
      585.0000000000        4.4351605237       -0.0005104735
      590.0000000000        3.4583946446       -0.0003058641
      595.0000000000        2.6954185108       -0.0001830127
      600.0000000000        2.1000040166       -0.0001093866
      605.0000000000        1.6357187042       -0.0000653284
      610.0000000000        1.2739157707       -0.0000389952
      615.0000000000        0.9921157415       -0.0000232702
```

620.0000000000	0.7727099835	-0.0000138858
625.0000000000	0.6019266231	-0.0000082874
630.0000000000	0.4690089647	-0.0000049480
635.0000000000	0.3655649868	-0.0000029559
640.0000000000	0.2850538529	-0.0000017672
645.0000000000	0.2223816672	-0.0000010575
650.0000000000	0.1735839801	-0.0000006335
655.0000000000	0.1355769450	-0.0000003799
660.0000000000	0.1059626331	-0.0000002282
665.0000000000	0.0828769582	-0.0000001372
670.0000000000	0.0648710464	-0.0000000827
675.0000000000	0.0508188015	-0.0000000499
680.0000000000	0.0398449524	-0.0000000302
685.0000000000	0.0312690880	-0.0000000183
690.0000000000	0.0245621569	-0.0000000111
695.0000000000	0.0193126719	-0.0000000067
700.0000000000	0.0152004650	-0.0000000041
705.0000000000	0.0119763108	-0.0000000025
710.0000000000	0.0094461087	-0.0000000015
715.0000000000	0.0074586050	-0.0000000009
720.0000000000	0.0058958616	-0.0000000006
725.0000000000	0.0046658559	-0.0000000004
730.0000000000	0.0036967351	-0.0000000002
735.0000000000	0.0029323524	-0.0000000001
740.0000000000	0.0023287986	-0.0000000001
745.0000000000	0.0018517066	-0.0000000001
750.0000000000	0.0014741535	-0.0000000000
755.0000000000	0.0011750297	-0.0000000000
760.0000000000	0.0009377678	-0.0000000000
765.0000000000	0.0007493528	-0.0000000000
770.0000000000	0.0005995502	-0.0000000000
775.0000000000	0.0004803041	-0.0000000000

UV/Vis Spectrum for $[RuCl_5]^-$

UV-VIS Spectrum# X-Axis: Excitation Energy (nm)
Y-Axis: Epsilon

# X	Y	DY/DX
380.0000000000	3364.8071764089	31.7456707514
385.0000000000	3593.1013003676	40.2358572304
390.0000000000	3848.8853575414	49.5031001876
395.0000000000	4121.5396269206	57.8904427175
400.0000000000	4400.4435759037	63.4781737183
405.0000000000	4675.4539486618	64.8450958717
410.0000000000	4937.3310784534	61.5486761495
415.0000000000	5178.0743633495	54.1922599989
420.0000000000	5391.1382702953	44.1372591338
425.0000000000	5571.5203820036	33.0339081812
430.0000000000	5715.7336579984	22.3624037162
435.0000000000	5821.6899584773	13.1211315885
440.0000000000	5888.5284124320	5.7143540401
445.0000000000	5916.4209428358	0.0171958338
450.0000000000	5906.3805820989	-4.4478278046
455.0000000000	5860.0890743292	-8.2984798584
460.0000000000	5779.7512431395	-12.1059851670
465.0000000000	5667.9764172474	-16.2693481199
470.0000000000	5527.6826114326	-20.9606602110
475.0000000000	5362.0171364422	-26.1321420717
480.0000000000	5174.2873389308	-31.5654137382
485.0000000000	4967.8965189257	-36.9411414247
490.0000000000	4746.2820134618	-41.9102793539
495.0000000000	4512.8543908184	-46.1538809583
500.0000000000	4270.9382899418	-49.4246828594
505.0000000000	4023.7164802448	-51.5689550374
510.0000000000	3774.1791822091	-52.5308130566
515.0000000000	3525.0806592424	-52.3432271583
520.0000000000	3278.9047014562	-51.1106063792
525.0000000000	3037.8400220168	-48.9874976595
530.0000000000	2803.7659121880	-46.1570412342
535.0000000000	2578.2478584099	-42.8117132560
540.0000000000	2362.5422851751	-39.1378101550
545.0000000000	2157.6091893291	-35.3042302467
550.0000000000	1964.1311855090	-31.4554467585
555.0000000000	1782.5373794852	-27.7081444519
560.0000000000	1613.0305043064	-24.1507763613
565.0000000000	1455.6158653002	-20.8452393522
570.0000000000	1310.1308148470	-17.8299165355
575.0000000000	1176.2736892866	-15.1234462098
580.0000000000	1053.6313653865	-12.7287156249
585.0000000000	941.7048146073	-10.6367184535
590.0000000000	839.9322372060	-8.8300417895
595.0000000000	747.7095369660	-7.2858536122
600.0000000000	664.4080469142	-5.9783423536
605.0000000000	589.3895357516	-4.8806174580
610.0000000000	522.0186150732	-3.9661166878
615.0000000000	461.6727314647	-3.2095863702
620.0000000000	407.7499687500	-2.5877089046
625.0000000000	359.6749078845	-2.0794513834
630.0000000000	316.9027991110	-1.6662032773
635.0000000000	278.9222966074	-1.3317622464
640.0000000000	245.2569931676	-1.0622170719
645.0000000000	215.4659742024	-0.8457666815
650.0000000000	189.1435887604	-0.6725050304

655.0000000000	165.9186121290	-0.5341936042
660.0000000000	145.4529512292	-0.4240366809
665.0000000000	127.4400214399	-0.3364692138
670.0000000000	111.6029023444	-0.2669631582
675.0000000000	97.6923606031	-0.2118550896
680.0000000000	85.4848109367	-0.1681958652
685.0000000000	74.7802711215	-0.1336216881
690.0000000000	65.4003539256	-0.1062450648
695.0000000000	57.1863279250	-0.0845636828
700.0000000000	49.9972699889	-0.0673850384
705.0000000000	43.7083247189	-0.0537646429
710.0000000000	38.2090800773	-0.0429557512
715.0000000000	33.4020636559	-0.0343687362
720.0000000000	29.2013603200	-0.0275384493
725.0000000000	25.5313491635	-0.0220981286
730.0000000000	22.3255556494	-0.0177586311
735.0000000000	19.5256133725	-0.0142919637
740.0000000000	17.0803289301	-0.0115182615
745.0000000000	14.9448428299	-0.0092955196
750.0000000000	13.0798791099	-0.0075115100
755.0000000000	11.4510763246	-0.0060774297
760.0000000000	10.0283927026	-0.0049229127
765.0000000000	8.7855785516	-0.0039921164
770.0000000000	7.6997093495	-0.0032406512
775.0000000000	6.7507733696	-0.0026331706

UV/Vis Spectrum for $[Ru_2Cl_6]^-$

```
# UV-VIS Spectrum
# X-Axis:  Excitation Energy (nm)
# Y-Axis:  Epsilon
#                  X                   Y                DY/DX
      380.0000000000     1259.4084809234      -12.8916765303
      385.0000000000     1117.6091083598       -3.7465438661
      390.0000000000     1019.7734212475        2.7753373780
      395.0000000000      957.7742012425        7.0528403620
      400.0000000000      923.5245418435        9.4617953489
      405.0000000000      909.5410291215       10.3525872551
      410.0000000000      909.2839880015       10.0577988635
      415.0000000000      917.3165235823        8.9005732795
      420.0000000000      929.3289511532        7.1913050396
      425.0000000000      942.0720484690        5.2132341099
      430.0000000000      953.2355797093        3.2040061760
      435.0000000000      961.3004084898        1.3410322438
      440.0000000000      965.3847232824       -0.2642739318
      445.0000000000      965.0981414427       -1.5622209829
      450.0000000000      960.4119769592       -2.5526644246
      455.0000000000      951.5497497384       -3.2688216592
      460.0000000000      938.8989633528       -3.7610848154
      465.0000000000      922.9431175077       -4.0837819669
      470.0000000000      904.2116692484       -4.2862925433
      475.0000000000      883.2450334127       -4.4085004993
      480.0000000000      860.5715509473       -4.4796354772
      485.0000000000      836.6935062414       -4.5191992350
      490.0000000000      812.0796185853       -4.5387877454
      495.0000000000      787.1618713850       -4.5439890349
      500.0000000000      762.3350045142       -4.5359577933
      505.0000000000      737.9574319184       -4.5125996339
      510.0000000000      714.3527294266       -4.4694819930
      515.0000000000      691.8111529349       -4.4006335375
      520.0000000000      670.5908919124       -4.2993461501
      525.0000000000      650.9189419838       -4.1590089144
      530.0000000000      632.9916017443       -3.9739271149
      535.0000000000      616.9746733911       -3.7400365540
      540.0000000000      603.0034848284       -3.4554204006
      545.0000000000      591.1828624469       -3.1205643373
      550.0000000000      581.5871772155       -2.7383311599
      555.0000000000      574.2605689075       -2.3136829414
      560.0000000000      569.2174294858       -1.8532157225
      565.0000000000      566.4432007595       -1.3645920847
      570.0000000000      565.8955160379       -0.8559597546
      575.0000000000      567.5056923798       -0.3354323421
      580.0000000000      571.1805601193        0.1893135774
      585.0000000000      576.8046001142        0.7112969642
      590.0000000000      584.2423466860        1.2243436915
      595.0000000000      593.3410053597        1.7230689962
      600.0000000000      603.9332289670        2.2027635072
      605.0000000000      615.8399930801        2.6592224454
      610.0000000000      628.8735116814        3.0885579998
      615.0000000000      642.8401360385        3.4870299800
      620.0000000000      657.5431835297        3.8509213583
      625.0000000000      672.7856482766        4.1764750509
      630.0000000000      688.3727515164        4.4598978603
      635.0000000000      704.1142963736        4.6974281664
      640.0000000000      719.8267987541        4.8854565745
      645.0000000000      735.3353732356        5.0206837285
```

650.0000000000	750.4753598344	5.1002969748
655.0000000000	765.0936841974	5.1221472986
660.0000000000	779.0499499493	5.0849095668
665.0000000000	792.2172674959	4.9882120932
670.0000000000	804.4828284675	4.8327253690
675.0000000000	815.7482391209	4.6202039719
680.0000000000	825.9296293921	4.3534797571
685.0000000000	834.9575569008	4.0364081064
690.0000000000	842.7767270857	3.6737720431
695.0000000000	849.3455518304	3.2711512832
700.0000000000	854.6355694996	2.8347647426
705.0000000000	858.6307492889	2.3712957001
710.0000000000	861.3267023007	1.8877088038
715.0000000000	862.7298208463	1.3910675290
720.0000000000	862.8563662409	0.8883596926
725.0000000000	861.7315238590	0.3863373295
730.0000000000	859.3884425418	-0.1086242123
735.0000000000	855.8672736489	-0.5906445907
740.0000000000	851.2142231838	-1.0544322746
745.0000000000	845.4806285587	-1.4953532115
750.0000000000	838.7220697211	-1.9094748667
755.0000000000	830.9975226010	-2.2935870696
760.0000000000	822.3685611645	-2.6452018072
765.0000000000	812.8986128047	-2.9625346052
770.0000000000	802.6522703806	-3.2444704320
775.0000000000	791.6946629358	-3.4905171851

UV/Vis Spectrum for $[Ru_2Cl_7]^-$

```
# UV-VIS Spectrum
# X-Axis:  Excitation Energy (nm)
# Y-Axis:  Epsilon
#                  X                    Y                DY/DX
      380.0000000000     5059.4104773827      -49.6430376457
      385.0000000000     4912.5950226685      -53.7824451716
      390.0000000000     4738.3067178342      -51.5613931279
      395.0000000000     4548.3562436307      -45.6456435899
      400.0000000000     4352.8573726913      -38.3950441125
      405.0000000000     4159.7379331313      -31.4251635736
      410.0000000000     3974.6726416136      -25.5656492999
      415.0000000000     3801.3055392353      -21.0472218486
      420.0000000000     3641.6313352595      -17.7520685783
      425.0000000000     3496.4287256261      -15.4230440595
      430.0000000000     3365.6709280778      -13.7936359866
      435.0000000000     3248.8698264692      -12.6454101275
      440.0000000000     3145.3352717922      -11.8179687673
      445.0000000000     3054.3487133698      -11.1963275894
      450.0000000000     2975.2609998809      -10.6925764553
      455.0000000000     2907.5294169262      -10.2302591880
      460.0000000000     2850.7105080285       -9.7343309586
      465.0000000000     2804.4244096755       -9.1269673591
      470.0000000000     2768.3043839481       -8.3286998314
      475.0000000000     2741.9426522917       -7.2641043255
      480.0000000000     2724.8409371075       -5.8709064887
      485.0000000000     2716.3715350746       -4.1108089714
      490.0000000000     2715.7524018710       -1.9798494141
      495.0000000000     2722.0376913352        0.4840400307
      500.0000000000     2734.1235040093        3.1982259568
      505.0000000000     2750.7672835028        6.0384354248
      510.0000000000     2770.6183609989        8.8477052888
      515.0000000000     2792.2565776144       11.4501539646
      520.0000000000     2814.2356821434       13.6676804721
      525.0000000000     2835.1282623773       15.3372716406
      530.0000000000     2853.5692636498       16.3266197146
      535.0000000000     2868.2956134983       16.5461582250
      540.0000000000     2878.1800403605       15.9562864561
      545.0000000000     2882.2577854816       14.5693189987
      550.0000000000     2879.7455077803       12.4464241421
      555.0000000000     2870.0522297589        9.6903959561
      560.0000000000     2852.7826395274        6.4354793314
      565.0000000000     2827.7334327376        2.8356206472
      570.0000000000     2794.8836426738       -0.9475278790
      575.0000000000     2754.3800698312       -4.7557175156
      580.0000000000     2706.5189936028       -8.4434817838
      585.0000000000     2651.7253420925      -11.8852650187
      590.0000000000     2590.5304277703      -14.9800941781
      595.0000000000     2523.5492433724      -17.6538547819
      600.0000000000     2451.4581700012      -19.8594340182
      605.0000000000     2374.9737919089      -21.5751244713
      610.0000000000     2294.8333517770      -22.8017444293
      615.0000000000     2211.7772256944      -23.5589360030
      620.0000000000     2126.5336552626      -23.8810645386
      625.0000000000     2039.8058497442      -23.8130770359
      630.0000000000     1952.2614663428      -23.4065972558
      635.0000000000     1864.5243923245      -22.7164522612
      640.0000000000     1777.1686882415      -21.7977476427
      645.0000000000     1690.7145055724      -20.7035420453
```

650.0000000000	1605.6257625997	-19.4831185765
655.0000000000	1522.3093469452	-18.1808119255
660.0000000000	1441.1156093821	-16.8353246866
665.0000000000	1362.3399189058	-15.4794526738
670.0000000000	1286.2250612982	-14.1401346609
675.0000000000	1212.9642805261	-12.8387445923
680.0000000000	1142.7047825121	-11.5915516645
685.0000000000	1075.5515426515	-10.4102838303
690.0000000000	1011.5712807332	-9.3027416794
695.0000000000	950.7964887540	-8.2734211251
700.0000000000	893.2294178273	-7.3241140659
705.0000000000	838.8459495075	-6.4544657009
710.0000000000	787.5992941107	-5.6624751960
715.0000000000	739.4234738471	-4.9449328650
720.0000000000	694.2365617718	-4.2977920092
725.0000000000	651.9436587455	-3.7164771950
730.0000000000	612.4395998931	-3.1961332325
735.0000000000	575.6113895961	-2.7318206550
740.0000000000	541.3403700340	-2.3186642902
745.0000000000	509.5041328800	-1.9519617425
750.0000000000	479.9781871385	-1.6272584334
755.0000000000	452.6373984777	-1.3403954012
760.0000000000	427.3572169070	-1.0875354608
765.0000000000	404.0147104551	-0.8651726319
770.0000000000	382.4894227336	-0.6701290392
775.0000000000	362.6640720667	-0.4995428023

UV/Vis Spectrum for $[Ru_3Cl_8]^-$

```
# UV-VIS Spectrum
# X-Axis:  Excitation Energy (nm)
# Y-Axis:  Epsilon
#                  X                    Y                DY/DX
      380.0000000000     3810.6101151390       15.9866533206
      385.0000000000     3820.1825464523       14.9886228833
      390.0000000000     3841.2635269324       13.2659948361
      395.0000000000     3865.8499987813       11.6673999635
      400.0000000000     3887.2202938971       10.3291846596
      405.0000000000     3900.0476080320        8.9147547110
      410.0000000000     3900.3758128155        6.9390417283
      415.0000000000     3885.5229153503        4.0413393820
      420.0000000000     3853.9508091747        0.1334376706
      425.0000000000     3805.1201559703       -4.5843906099
      430.0000000000     3739.3379561991       -9.7031274549
      435.0000000000     3657.6010249020      -14.7280701369
      440.0000000000     3561.4384051891      -19.1985158467
      445.0000000000     3452.7571268784      -22.7740898146
      450.0000000000     3333.6968866746      -25.2761531861
      455.0000000000     3206.4993644051      -26.6872446825
      460.0000000000     3073.3969078597      -27.1200995107
      465.0000000000     2936.5235545675      -26.7707831312
      470.0000000000     2797.8492966134      -25.8693385773
      475.0000000000     2659.1365720123      -24.6378132326
      480.0000000000     2521.9164775373      -23.2611541498
      485.0000000000     2387.4812738214      -21.8723928811
      490.0000000000     2256.8893875234      -20.5504780662
      495.0000000000     2130.9792107329      -19.3273272876
      500.0000000000     2010.3884157010      -18.2000921177
      505.0000000000     1895.5761004938      -17.1449790330
      510.0000000000     1786.8457359114      -16.1298715998
      515.0000000000     1684.3675060157      -15.1240992028
      520.0000000000     1588.1991681896      -14.1047211173
      525.0000000000     1498.3049781570      -13.0594788947
      530.0000000000     1414.5725278803      -11.9870561826
      535.0000000000     1336.8275416171      -10.8954928246
      540.0000000000     1264.8467873229       -9.7995941164
      545.0000000000     1198.3693091422       -8.7180364298
      550.0000000000     1137.1061927523       -7.6706708859
      555.0000000000     1080.7490563683       -6.6763232903
      560.0000000000     1028.9774296646       -5.7512158400
      565.0000000000      981.4651500038       -4.9080097498
      570.0000000000      937.8858758655       -4.1553894242
      575.0000000000      897.9177940842       -3.4980710400
      580.0000000000      861.2475812450       -2.9371106407
      585.0000000000      827.5736698437       -2.4703979832
      590.0000000000      796.6088653737       -2.0932430699
      595.0000000000      768.0823598541       -1.7989857151
      600.0000000000      741.7411889799       -1.5795803634
      605.0000000000      717.3511827701       -1.4261265391
      610.0000000000      694.6974623164       -1.3293291108
      615.0000000000      673.5845372900       -1.2798822888
      620.0000000000      653.8360598300       -1.2687776576
      625.0000000000      635.2942901355       -1.2875404362
      630.0000000000      617.8193275029       -1.3284003378
      635.0000000000      601.2881578240       -1.3844044740
      640.0000000000      585.5935648861       -1.4494801634
      645.0000000000      570.6429484334       -1.5184555221
```

650.0000000000	556.3570871098	-1.5870455100
655.0000000000	542.6688793327	-1.6518107367
660.0000000000	529.5220900638	-1.7100958521
665.0000000000	516.8701265009	-1.7599537608
670.0000000000	504.6748610548	-1.8000612267
675.0000000000	492.9055156920	-1.8296306934
680.0000000000	481.5376178758	-1.8483223617
685.0000000000	470.5520349528	-1.8561597611
690.0000000000	459.9340909310	-1.8534512722
695.0000000000	449.6727671478	-1.8407193123
700.0000000000	439.7599863274	-1.8186382284
705.0000000000	430.1899779269	-1.7879813568
710.0000000000	420.9587214375	-1.7495772227
715.0000000000	412.0634633938	-1.7042744713
720.0000000000	403.5023032131	-1.6529148376
725.0000000000	395.2738425811	-1.5963132743
730.0000000000	387.3768929031	-1.5352442507
735.0000000000	379.8102352870	-1.4704331976
740.0000000000	372.5724276100	-1.4025520960
745.0000000000	365.6616533928	-1.3322182661
750.0000000000	359.0756074548	-1.2599955105
755.0000000000	352.8114136227	-1.1863968691
760.0000000000	346.8655700947	-1.1118883679
765.0000000000	341.2339184117	-1.0368932587
770.0000000000	335.9116323456	-0.9617963625
775.0000000000	330.8932233646	-0.8869482317

UV/Vis Spectrum for $[Ru_3Cl_9]^-$

```
# UV-VIS Spectrum
# X-Axis:  Excitation Energy (nm)
# Y-Axis:  Epsilon
#                  X                    Y                DY/DX
      380.0000000000     7006.6009759427      -50.3660753012
      385.0000000000     6673.5474337694      -45.3718865609
      390.0000000000     6348.2764165427      -42.3258560317
      395.0000000000     6032.3155504784      -40.9122108162
      400.0000000000     5726.4708218553      -40.3479899755
      405.0000000000     5431.0050187223      -39.8904504230
      410.0000000000     5145.8484586503      -39.1184209338
      415.0000000000     4870.7811933299      -37.9699408441
      420.0000000000     4605.5628025923      -36.6182547569
      425.0000000000     4350.0088631702      -35.2980036922
      430.0000000000     4104.0241967218      -34.1692927994
      435.0000000000     3867.6060475821      -33.2594680625
      440.0000000000     3640.8291623902      -32.4781400765
      445.0000000000     3423.8219786075      -31.6752832101
      450.0000000000     3216.7402495644      -30.7072069753
      455.0000000000     3019.7420559699      -29.4845472029
      460.0000000000     2832.9664026066      -27.9912747778
      465.0000000000     2656.5163881824      -26.2768736329
      470.0000000000     2490.4471321317      -24.4315968568
      475.0000000000     2334.7581318020      -22.5566464305
      480.0000000000     2189.3894288388      -20.7388440945
      485.0000000000     2054.2208316521      -19.0351305643
      490.0000000000     1929.0734307413      -17.4679885523
      495.0000000000     1813.7127185441      -16.0298050111
      500.0000000000     1707.8527505100      -14.6926575371
      505.0000000000     1611.1609279486      -13.4198506018
      510.0000000000     1523.2631207732      -12.1762777315
      515.0000000000     1443.7489625476      -10.9358382083
      520.0000000000     1372.1772327444       -9.6852840134
      525.0000000000     1308.0812906826       -8.4247654055
      530.0000000000     1250.9745464893       -7.1658848452
      535.0000000000     1200.3559539151       -5.9282746081
      540.0000000000     1155.7154962238       -4.7356627637
      545.0000000000     1116.5396173523       -3.6121859522
      550.0000000000     1082.3165322013       -2.5794383826
      555.0000000000     1052.5413364008       -1.6544843818
      560.0000000000     1026.7208293686       -0.8488489622
      565.0000000000     1004.3779654678       -0.1683551506
      570.0000000000      985.0558558963        0.3864018833
      575.0000000000      968.3212571591        0.8191766034
      580.0000000000      953.7674988263        1.1370061642
      585.0000000000      941.0168219459        1.3491289580
      590.0000000000      929.7221183587        1.4660117657
      595.0000000000      919.5680789531        1.4985579260
      600.0000000000      910.2717746487        1.4575252367
      605.0000000000      901.5827070340        1.3531489043
      610.0000000000      893.2823758134        1.1949425639
      615.0000000000      885.1834175191        0.9916383102
      620.0000000000      877.1283744685        0.7512229355
      625.0000000000      868.9881549786        0.4810299434
      630.0000000000      860.6602457375        0.1878531638
      635.0000000000      852.0667353645       -0.1219439806
      640.0000000000      843.1522049434       -0.4423408376
      645.0000000000      833.8815370487       -0.7676027815
```

650.0000000000	824.2376898269	-1.0922579058
655.0000000000	814.2194773158	-1.4111046164
660.0000000000	803.8393916309	-1.7192441934
665.0000000000	793.1214971012	-2.0121305385
670.0000000000	782.0994210466	-2.2856287832
675.0000000000	770.8144607792	-2.5360748788
680.0000000000	759.3138216493	-2.7603294280
685.0000000000	747.6489966095	-2.9558205471
690.0000000000	735.8742938641	-3.1205722367
695.0000000000	724.0455157255	-3.2532163894
700.0000000000	712.2187888050	-3.3529880406
705.0000000000	700.4495431243	-3.4197046979
710.0000000000	688.7916356172	-3.4537315092
715.0000000000	677.2966117689	-3.4559346669
720.0000000000	666.0130977999	-3.4276257916
725.0000000000	654.9863147848	-3.3705001505
730.0000000000	644.2577053905	-3.2865714773
735.0000000000	633.8646634768	-3.1781059279
740.0000000000	623.8403565922	-3.0475573694
745.0000000000	614.2136313861	-2.8975058155
750.0000000000	605.0089921206	-2.7306004038
755.0000000000	596.2466427548	-2.5495079160
760.0000000000	587.9425834836	-2.3568674642
765.0000000000	580.1087531035	-2.1552516388
770.0000000000	572.7532091332	-1.9471341389
775.0000000000	565.8803382141	-1.7348636780

UV/Vis Spectrum for $[Ru_4Cl_{11}]^-$

 # UV-VIS Spectrum
X-Axis: Excitation Energy (nm)
Y-Axis: Epsilon

# X	Y	DY/DX
380.0000000000	3799.5886263160	-22.2772890951
385.0000000000	3605.4883822010	-7.2879507399
390.0000000000	3481.7461566499	4.0218880255
395.0000000000	3418.0181080870	11.8422417792
400.0000000000	3403.9143868391	16.6719599995
405.0000000000	3429.7123051134	19.1881527644
410.0000000000	3486.8022434648	20.1206397709
415.0000000000	3567.9101922552	20.1412107920
420.0000000000	3667.1493086753	19.7803612142
425.0000000000	3779.9519567221	19.3831522040
430.0000000000	3902.9268058799	19.1090499230
435.0000000000	4033.6759530710	18.9704589502
440.0000000000	4170.5972319518	18.8955312651
445.0000000000	4312.6884663570	18.7962469840
450.0000000000	4459.3640963019	18.6239513375
455.0000000000	4610.2903566453	18.4003930381
460.0000000000	4765.2426092459	18.2203807919
465.0000000000	4923.9869498038	18.2298278131
470.0000000000	5086.1872927342	18.5882724441
475.0000000000	5251.3383849413	19.4271141749
480.0000000000	5418.7243938415	20.8139661305
485.0000000000	5587.4017988576	22.7305516833
490.0000000000	5756.2043449406	25.0675926785
495.0000000000	5923.7669050332	27.6362128934
500.0000000000	6088.5643670129	30.1922951017
505.0000000000	6248.9612032764	32.4683996781
510.0000000000	6403.2672456692	34.2073450849
515.0000000000	6549.7953737578	35.1921679887
520.0000000000	6686.9172876134	35.2685686256
525.0000000000	6813.1142062166	34.3577006796
530.0000000000	6927.0201249201	32.4589148259
535.0000000000	7027.4560961555	29.6435317199
540.0000000000	7113.4547933899	26.0417382145
545.0000000000	7184.2753229200	21.8252164304
550.0000000000	7239.4088246203	17.1881668765
555.0000000000	7278.5758334901	12.3290733614
560.0000000000	7301.7166573890	7.4350077474
565.0000000000	7308.9761739552	2.6696173542
570.0000000000	7300.6844810250	-1.8347107029
575.0000000000	7277.3347741168	-5.9805734160
580.0000000000	7239.5596971067	-9.7056509839
585.0000000000	7188.1072422257	-12.9799346815
590.0000000000	7123.8170841064	-15.8009559530
595.0000000000	7047.5980370348	-18.1878844665
600.0000000000	6960.4071378887	-20.1752674273
605.0000000000	6863.2306884344	-21.8070310564
610.0000000000	6757.0674451022	-23.1311894366
615.0000000000	6642.9140244427	-24.1955314254
620.0000000000	6521.7524982687	-25.0444010921
625.0000000000	6394.5400824260	-25.7165618590
630.0000000000	6262.2007745745	-26.2440435391
635.0000000000	6125.6187660897	-26.6518141443
640.0000000000	5985.6334378136	-26.9580907352
645.0000000000	5843.0357455957	-27.1750998734

650.0000000000	5698.5658063408	-27.3101119214
655.0000000000	5552.9115060031	-27.3665982645
660.0000000000	5406.7079654309	-27.3453910614
665.0000000000	5260.5377164403	-27.2457570229
670.0000000000	5114.9314576281	-27.0663268384
675.0000000000	4970.3692762771	-26.8058481822
680.0000000000	4827.2822385864	-26.4637516762
685.0000000000	4686.0542649896	-26.0405354521
690.0000000000	4547.0242202872	-25.5379852588
695.0000000000	4410.4881596663	-24.9592539892
700.0000000000	4276.7016814512	-24.3088277983
705.0000000000	4145.8823457320	-23.5924064789
710.0000000000	4018.2121250117	-22.8167242324
715.0000000000	3893.8398588537	-21.9893341278
720.0000000000	3772.8836893810	-21.1183759627
725.0000000000	3655.4334585257	-20.2123433862
730.0000000000	3541.5530513061	-19.2798623582
735.0000000000	3431.2826722429	-18.3294895229
740.0000000000	3324.6410444225	-17.3695360155
745.0000000000	3221.6275227636	-16.4079196583
750.0000000000	3122.2241148146	-15.4520464502
755.0000000000	3026.3974039547	-14.5087206938
760.0000000000	2934.1003712420	-13.5840819762
765.0000000000	2845.2741133650	-12.6835664757
770.0000000000	2759.8494552444	-11.8118896291
775.0000000000	2677.7484568096	-10.9730470083

UV/Vis Spectrum for $[Ru_5Cl_{12}]^-$

```
# UV-VIS Spectrum
# X-Axis:  Excitation Energy (nm)
# Y-Axis:  Epsilon
#                  X                    Y                DY/DX
      380.0000000000     7459.1504569778      -40.4004814553
      385.0000000000     7154.4489678452      -35.8170427553
      390.0000000000     6867.6825942214      -32.5900714482
      395.0000000000     6597.2147088760      -30.4856009592
      400.0000000000     6341.1226821284      -29.2263709964
      405.0000000000     6097.5216813398      -28.5777157218
      410.0000000000     5864.7785560496      -28.3704193522
      415.0000000000     5641.6321116545      -28.4820990631
      420.0000000000     5427.2386277608      -28.8049329100
      425.0000000000     5221.1616293151      -29.2210906694
      430.0000000000     5023.3234621217      -29.5956132141
      435.0000000000     4833.9338522149      -29.7859188180
      440.0000000000     4653.4078607334      -29.6608353261
      445.0000000000     4482.2828309789      -29.1205185932
      450.0000000000     4321.1412760883      -28.1105211652
      455.0000000000     4170.5442958542      -26.6267301253
      460.0000000000     4030.9781027608      -24.7112648875
      465.0000000000     3902.8146059607      -22.4417395651
      470.0000000000     3786.2857476221      -19.9172624548
      475.0000000000     3681.4703891506      -17.2443733533
      480.0000000000     3588.2919701390      -14.5252496449
      485.0000000000     3506.5248642507      -11.8494034739
      490.0000000000     3435.8072806921       -9.2890900598
      495.0000000000     3375.6586527391       -6.8979382463
      500.0000000000     3325.4996636142       -4.7119443373
      505.0000000000     3284.6733382614       -2.7518900997
      510.0000000000     3252.4659384722       -1.0263623937
      515.0000000000     3228.1267083303        0.4652323517
      520.0000000000     3210.8858056470        1.7300292839
      525.0000000000     3199.9700092951        2.7796063112
      530.0000000000     3194.6160049468        3.6284383275
      535.0000000000     3194.0812205911        4.2928250144
      540.0000000000     3197.6523098796        4.7901712639
      545.0000000000     3204.6514697596        5.1384952502
      550.0000000000     3214.4408343009        5.3560583591
      555.0000000000     3226.4252149371        5.4610413157
      560.0000000000     3240.0534643689        5.4712228492
      565.0000000000     3254.8187325237        5.4036452778
      570.0000000000     3270.2578630579        5.2742724807
      575.0000000000     3285.9501519663        5.0976589353
      580.0000000000     3301.5156592598        4.8866543395
      585.0000000000     3316.6132329486        4.6521681354
      590.0000000000     3330.9383736650        4.4030136861
      595.0000000000     3344.2210395084        4.1458446561
      600.0000000000     3356.2234649727        3.8851878551
      605.0000000000     3366.7380455942        3.6235687011
      610.0000000000     3375.5853214002        3.3617184549
      615.0000000000     3382.6120772868        3.0988470569
      620.0000000000     3387.6895668845        2.8329620357
      625.0000000000     3390.7118579413        2.5612125515
      630.0000000000     3391.5942913806        2.2802380198
      635.0000000000     3390.2720425445        1.9865025974
      640.0000000000     3386.6987712969        1.6765997305
      645.0000000000     3380.8453472365        1.3475145555
```

650.0000000000	3372.6986368958	0.9968358252
655.0000000000	3362.2603411514	0.6229128773
660.0000000000	3349.5458728858	0.2249567095
665.0000000000	3334.5832669801	-0.1969127179
670.0000000000	3317.4121168153	-0.6416683689
675.0000000000	3298.0825334796	-1.1074208200
680.0000000000	3276.6541257191	-1.5914981908
685.0000000000	3253.1950002691	-2.0905531904
690.0000000000	3227.7807835330	-2.6006890953
695.0000000000	3200.4936666061	-3.1175968478
700.0000000000	3171.4214763948	-3.6366961554
705.0000000000	3140.6567760616	-4.1532743889
710.0000000000	3108.2959982641	-4.6626181301
715.0000000000	3074.4386146800	-5.1601333217
720.0000000000	3039.1863451624	-5.6414510658
725.0000000000	3002.6424095699	-6.1025171464
730.0000000000	2964.9108249180	-6.5396642795
735.0000000000	2926.0957500163	-6.9496669038
740.0000000000	2886.3008792289	-7.3297789902
745.0000000000	2845.6288864447	-7.6777558849
750.0000000000	2804.1809197961	-7.9918615933
755.0000000000	2762.0561471254	-8.2708631888
760.0000000000	2719.3513516969	-8.5140141878
765.0000000000	2676.1605771880	-8.7210287991
770.0000000000	2632.5748205790	-8.8920489428
775.0000000000	2588.6817711962	-9.0276058549